Chemical composition, optical properties, and oxidative potential of water- and methanol-soluble organic compounds emitted from the combustion of biomass materials and coal

Tao Cao[1,3], Meiju Li[1,3], Chunlin Zou[1,3], Xingjun Fan[4], Jianzhong Song[1,2,5,*], Wanglu, Jia[1,2], Chiling Yu[1,2], Zhiqiang Yu[1,2], Ping'an Peng[1,2,3,5]

[1]State Key Laboratory of Organic Geochemistry and Guangdong Provincial Key Laboratory of Environmental Protection and Resources Utilization, Guangzhou Institute of Geochemistry, Chinese Academy of Sciences, Guangzhou 510640, China

[2]CAS Center for Excellence in Deep Earth Science, Guangzhou, 510640, China

[3]University of Chinese Academy of Sciences, Beijing 100049, China

[4]College of Resource and Environment, Anhui Science and Technology University, Anhui 233100, China

[5]Guangdong-Hong Kong-Macao Joint Laboratory for Environmental Pollution and Control

*_Correspondence to_: Jianzhong Song (songjzh@gig.ac.cn)

Abstract

Biomass burning (BB) and coal combustion (CC) are important sources of brown carbon (BrC) in ambient aerosols. In this study, six biomass materials and five types of coal were combusted to generate fine smoke particles. The BrC fractions, including water-soluble organic carbon (WSOC), humic-like substance-carbon (HULIS-C), and methanol-soluble organic carbon (MSOC), were subsequently fractionated, and their optical properties and chemical structures were then comprehensively investigated using UV-visible spectroscopy, proton nuclear magnetic resonance spectroscopy (^{1}H-NMR), and fluorescence extraction-emission matrix spectroscopy (EEM) combined with parallel factor analysis (PARAFAC). In addition, the oxidative potential (OP) of BB and CC BrC was measured with the dithiothreitol (DTT) method. The results showed that WSOC, HULIS-C, and MSOC accounted for 2.3%–22%, 0.5%–10%, and 6.4%–73% of the total mass of combustion-derived smoke $PM_{2.5}$, respectively, with MSOC extracting the highest concentrations of organic compounds. The MSOC fractions had the highest light absorption capacity (mass absorption efficiency at 365 nm ((MAE_{365}): 1.0–2.7 m^2/gC) for both BB and CC smoke, indicating that MSOC contained more of the strong light-absorbing components. Therefore, MSOC may represent the total BrC better than the water-soluble fractions. Some significant differences were observed between the BrC fractions emitted from BB and CC with more water-soluble BrC fractions with higher MAE_{365} and lower absorption Ångström exponent values detected in smoke emitted from BB than from CC. EEM-PARAFAC identified four fluorophores: two protein-like, one humic-like, and one polyphenol-like. The protein-like substances were the dominant components of WSOC (47%–80%), HULIS-C

(44%–87%), and MSOC (42%–70%). The ^{1}H-NMR results suggested that BB BrC contained more oxygenated aliphatic functional groups (H-C-O) whereas CC BrC contained more unsaturated fractions (H-C-C = and Ar-H). The DTT assays indicated that BB BrC generally had a stronger oxidative potential (DTT_m, 2.6–85 pmol/min/μg) than CC BrC (DTT_m, 0.4–11 pmol/min/μg), with MSOC having a stronger OP than WSOC and HULIS-C. Furthermore, the Principal component analysis and Pearson correlation coefficients indicated that highly oxygenated humic-like fluorophore C4 may be the important DTT active substances in BrC.

1. Introduction

Brown carbon (BrC) is an organic compound with strong light absorption at ultraviolet and short visible wavelengths and is abundant in ambient aerosols (Chen and Bond, 2010; Laskin et al., 2015; Alexander et al., 2008), rain, clouds, and fog water (Santos et al., 2009; Santos et al., 2012; Izhar et al., 2020). Due to its strong light absorption ability, BrC can affect the radiative balance of aerosol and photochemical reactions in the atmospheric environment (Andreae and Gelencser, 2006; Kumar et al., 2018a; Nozière et al., 2011). Moreover, BrC has the ability to catalyze the generation of reactive oxygen species (ROS), which potentially have an adverse impact on human health (Bates et al., 2019; Ma et al., 2018; Fan et al., 2018; Chen et al., 2019).

Brown carbon originates from various sources, including primary emission sources, such as biomass burning (BB), coal combustion (CC), and vehicular emissions (Fan et al., 2018; Li et al., 2018; Chen et al., 2019; Sun et al., 2017); and secondary processes, such as reactions between carbonyls and ammonia or amines and the photochemical transformation of volatile organic compounds (Evangeliou et al., 2019; Lin et al., 2015). Among these sources, BB and CC are considered to make significant contributions to atmospheric BrC materials as indicated in both laboratory and field studies (Li et al., 2018; Park and Yu, 2016; van der Werf et al., 2010; Yan et al., 2015). For example, BrC fractions, such as water-soluble organic carbon (WSOC), humic-like substance-carbon (HULIS-C), and methanol-soluble organic carbon (MSOC), have been found to be abundant in fresh emissions from the burning of crop straw, wood branches, and coals (Park and Yu, 2016; Fan et al., 2018; Li et al., 2018; Huo et al., 2018). These studies have also demonstrated that the chemical properties of primary BrC

are variable due to the inherent heterogeneity and complexity of fuel materials and combustion conditions (Huo et al., 2018; Fan et al., 2018; Li et al., 2018; Atwi et al., 2021). For example, the light absorption properties of primary HULIS-C produced by the combustion of three types of crop straw under different moisture contents and stacking modes are different. The absorption Ångström exponent (AAE) increased and the mass absorption efficiency at 365 nm (MAE_{365}) decreased under high moisture or stacking conditions (Huo et al., 2018). The water-soluble BrC emitted from low maturity CC generally had relatively low MAE_{365} values (Li et al., 2018). However, most of these studies only focused on the relative abundances, chemical composition, and optical properties of water-soluble BrC (e.g., HULIS) emitted from the combustion of various fuels and different combustion conditions (e.g., smoldering and flaming) (Huo et al., 2018; Park et al., 2016; Fan et al., 2016). It is noted that water-insoluble BrC even exhibits a higher light absorption than water-soluble BrC in ambient aerosols (Chen et al., 2016, 2017; Bai et al., 2020; Huang et al., 2020; Li et al., 2019). However, knowledge on the chemical and optical properties of water-insoluble BrC from combustion sources is still lacking. Moreover, the association of chemical compositions responsible for light absorption of BrC from combustion sources is still constrained. Therefore, to gain more detailed information on BrC from combustion sources, a comprehensive characterization, including the chemical and optical characteristics of the BrC fractions (including both water-soluble and water-insoluble BrC) from the combustion of biomass materials and coals, is required.

In addition, the oxidative potential (OP) of water-soluble organic fractions (WSOC and HULIS) and the water-insoluble organic fraction in ambient aerosols have been investigated,

and all are known to be significant redox-active organic compounds associated with ROS generation, which can adversely affect human health (Moufarrej et al., 2020; Bates et al., 2019; Verma et al., 2012; Kramer et al., 2016; Wong et al., 2019). As important contributors to ambient BrC, combustion-derived BrC is expected to have a strong ROS generation capacity and be harmful to human health. Verma et al. (2014) analyzed the potential of the water-soluble fraction of atmospheric fine aerosols in the southeastern United States to generate ROS and revealed that biomass burning dominates the ROS-generation potential in winter, contributing more than 46% to DTT activities. In addition, study on the oxidative potential of water-soluble HULIS in fine aerosols in Beijing also indicated that combustion sources contributed a high proportion to the oxidative stress of water-soluble HULIS fractions (Ma et al., 2018). However, these results were mainly obtained based on the source apportionment receptor model (positive matrix factorization (PMF) and chemical mass balances (CMB)). Recently, the water extracts and HULIS from biomass burning were directly investigated and presented significant oxidative potential to generate ROS (e.g., 6.6-10.7 pmol/min/μg for HULIS) (Fan et al., 2018). However, this limited studies only focused on the water-soluble BrC fraction from biomass burning; and knowledge on the oxidative potential of the water-insoluble BB BrC and BrC fractions emitted from other combustion processes, such as coal combustion, is still lacking. In addition, the DTT activities of BrC from different combustion sources were generally different, but the key components or functional groups that responsible for the ROS generation capacity of combustion-derived BrC are unclear.

Biomass fuels and coals are two traditional sources of energy in residential properties in

some developing countries, especially China and India (Sun et al., 2017; Huo et al., 2018; Singh et al., 2021). Due to incomplete combustion and poor pollution control, BB and CC release various pollutants, including particulate matter (PM), elemental carbon (EC), and BrC. In this study, we investigated the optical properties, chemical composition, and oxidative potential of BrC fractions in smokes emitted from BB and CC. Six biomass materials (three types of crop straw and three types of wood branches) and five coals with different maturities were combusted, and the resulting smoke particles were collected in a laboratory combustion chamber. The water soluble (WSOC and HULIS-C) and methanol soluble (MSOC) fractions in smoke were fractionated using pure water combined with solid-phase extraction (SPE) and methanol extraction. Subsequently, their chemical and optical properties were measured using a total organic carbon analyzer, UV-visible spectroscopy, fluorescence extraction-emission matrix spectroscopy (EEM) combined with parallel factor analysis (PARAFAC), and proton nuclear magnetic resonance spectroscopy (^{1}H-NMR). Moreover, the oxidative potential of the BrC fractions was determined by a dithiothreitol (DTT) assay. This is a comprehensive study of the chemical and optical properties of BrC fractions, including both water-soluble and water-insoluble fractions from BB and CC. The OP of different BrC fractions from BB and CC were directly determined, and the key components or properties associated with the OP of BrC were further discussed. The information obtained will enhance our understanding of the chemical composition, light absorption, fluorophores, and DTT activity of the primary BrC from BB and CC and could be used to estimate the environmental and climate impacts of different types of combustion-derived BrC.

2. Materials and methods

2.1. The BB and CC smoke samples

In this study, six biomass materials and five types of coal were collected and used to generate smoke samples. The biomass materials consisted of three types of crop straw (wheat straw (WS), rice straw (RS), and corn straw (CS)) and three types of wood branches (pine wood (PW), Chinese fir (CF), and white poplar (WP)). These materials are usually used as fuels for heating and cooking in rural areas and are also occasionally burned in the field (Fan et al., 2018; Kumar et al., 2018b). The combustion of these crop straws and woody fuels is reported to make a significant contribution to atmospheric aerosols in China (Shen et al., 2013). Five types of coal were used for the collection of CC smoke samples. They consisted of four types of bituminous coal (B-1, B-2, B-3, and B-4) and one anthracite coal (AN), representing the major types of coal used for residential CC in China. The details of these samples are provided in the supporting information (SI).

Samples of the smoke emitted from BB and CC were collected in a combustion and sampling system. The system consisted of a combustion hood, clean background air dilution and injection ports, smoke pipe, mixing fan, mixing chamber, $PM_{2.5}$ sampler (JCH-120F, Juchuang Environmental Protection Group Co., Ltd., Shandong, China), and an exhaust port. The details of the sampling procedure are described in our previous study (Fan et al., 2018; Li et al., 2018) and the SI file.

Blank quartz filters were collected before each group of combustion experiments prior to the fuels being ignited. Blank filters were used to correct the mass of smoke, the optical signals and DTT consumption by BrC. To prevent contamination of the following sample, the

161 collection system was cleaned before each new combustion experiment.

162

163 **2.2. Extraction and isolation of BrC fractions**

164 In this study, the WSOC, HULIS-C, and MSOC fractions were obtained using the
165 solvent extraction method, as described in our previous studies (Fan et al., 2016; Li et al.,
166 2018). Initially, the filter samples were cut into small pieces and ultrasonically extracted three
167 times with 20 mL ultrapure water for 30 min. The extract was filtered through a 0.22 μm
168 polytetrafluoroethylene (PTFE) syringe filter (Jinteng, Tianjin, China), which collected the
169 WSOC fraction. The HULIS-C fraction in WSOC was further isolated using the SPE (Oasis
170 HLB, 200 mg, Waters, Milford, MA, USA) method. The detailed procedure is provided in S3
171 of SI file.

172 The MSOC fraction was obtained using a method developed by Cheng et al. (2016).
173 Briefly, a portion of the filter was immersed in methanol (Macklin, >99.9%, Shanghai, China)
174 for 2 h and then filtered through a 0.22 μm PTFE syringe filter. Static digestion without
175 ultrasonic treatment can avoid the loss of PM and facilitate the determination of the dissolved
176 organic matter (DOM) content. Finally, the residual filters were dried in a vacuum dryer. The
177 OC content of MSOC was obtained by subtracting the OC concentration of the extracted
178 filters from untreated filters.

179

180 **2.3. UV-visible spectroscopy**

181 The UV-visible absorption spectra of the BrC solutions were analyzed using a UV-vis
182 spectrophotometer (UV-2600, Shimadzu, Kyoto, Japan). The BrC solution was placed in a

183 0.01 m quartz cuvette, and the UV-vis spectra were recorded from 200 to 700 nm at 1 nm
184 intervals. Milli-Q water was used as a blank reference for the WSOC and HULIS-C solutions
185 while pure methanol was used as the blank for the MSOC fraction. The corresponding
186 background was used to determine the interference from the instrument and operational blank
187 sample.

188 To describe the optical properties of BrC fractions, the AAE and MAE_{365} were
189 calculated in this study. The AAE is a measure of the spectral dependence of chromophores in
190 BrC while the MAE_{365} can indicate the light absorbing capacity of BrC (Fan et al., 2016;
191 Cheng et al., 2016). The detailed calculations are described in the SI file.

192

193 **2.4. Fluorescence EEM spectroscopy and the PARAFAC model**

194 The EEM fluorescence spectra of BrC fractions were recorded by an F-4600
195 fluorescence spectrometer (Hitachi, Tokyo, Japan) using a 0.01 m width quartz cuvette with a
196 400 V xenon lamp at room temperature and a 2400 nm/min scanning speed. The scanning
197 ranges for excitation (E_X) and emission (E_M) were 200–400 nm and 290–520 nm, respectively.
198 The slit width and intervals for E_X and E_M were both set to 5 nm. According to the different
199 solvents used for sample extraction (water and methanol), all EEM spectra were divided into
200 two groups for analysis (66 samples for water-soluble WSOC and HULIS-C and 33 samples
201 for MSOC). The PARAFAC modeling procedure was conducted in EFC v1.2, which is an
202 application software based on MATLAB that has the functions of conversion, correction,
203 cognition, comparison, and calculation for processing the fluorescence spectra (He and Hur,
204 2015; Murphy et al., 2011; Murphy et al., 2013). The PARAFAC analysis method that was

included in the software was consistent with the calculation made by the drEEM toolkit when using MATLAB (Murphy et al., 2010; Murphy et al., 2013). The PARAFAC was computed using two to seven component models, with nonnegativity constraints and a residual analysis; and split half analysis was used to validate the number of fluorescence components. According to the results of the split-half and core consistency analysis, four component models were chosen for both the WSOC and HULIS-C fractions and the MSOC. The EEM was normalized to the area under the ultrapure water Raman peak (E_X = 350 nm, E_M = 365–430 nm) collected before the measurement of samples to produce corrected fluorescence intensities in Raman units (Lawaetz and Stedmon, 2009). The relative contribution of individual chromophores was estimated by calculating the maximum fluorescence intensities (F_{max}: maximum fluorescence intensity of identified fluorescence components, relative content % = $F_{max}/\Sigma F_{max}$) (Matos et al., 2015; Chen et al., 2016).

2.5. Proton-NMR spectroscopy

Approximately 5 mg of the BrC fractions (i.e., HULIS-C, WSOC, and MSOC) derived from BB and CC were used for ^{1}H NMR measurements. The water-soluble BrC fractions (WSOC and HULIS-C) were redissolved in 500 μL deuterium oxide, and MSOC was redissolved in 500 μL deuterated methanol and then transferred to a 5 mm NMR tube. ^{1}H-NMR spectra were obtained at a frequency of 400 MHz using a spectrometer (Avance III 400, Bruker Daltonik GmbH, Bremen, Germany). Data were acquired from 100 scans, with a recycling time of 2 s for a condensed water sample. The length of the proton 90° pulse was 8.87 μs. A 1.0 Hz line-broadening weighting function and baseline correction were applied.

The identification of the functional groups in the NMR spectra was based on their chemical shift (δH) relative to that of tetramethylsilane (0 ppm), which was applied as an internal standard (Zou et al., 2020).

2.6. Oxidative potential

The oxidative potential of BrC emitted from the BB and CC processes (i.e., WSOC, HULIS-C, and MSOC) was measured by a DTT assay. This protocol was mainly followed the methods introduced by Fan et al (2018) and Gao et al (2020), and also with some minor modifications. Briefly, 3 mL of extracted sample solution (MSOC was a mixture of 100 μL sample and 2.9 mL of 18.2 MΩ Milli-Q water, and the corresponding blank was the same solution as that of the water blank) and 3 mL of 1 mM DTT were mixed in a 20 mL brown vial and then placed in a 37 °C water bath to maintain the samples at a constant temperature. At specific time intervals (0, 5, 10, 15, and 20 min), 1 mL of the well-mixed sample was transferred to another 4 mL brown vial, and 1 ml trichloroacetic acid (TCA 1% w/v) was added to stop the reaction. Then, 0.5 mL 5,5'-dithiobis-(2-nitrobenzoic acid) (DTNB, 1 mM) was added to react with the remaining DTT to produce 2-nitro-5-thiobenzoic acid (TNB). After 5 min, 1 mL of tris(hydroxymethyl)methyl aminomethane buffer (0.4 mM Tris buffer, pH 8.9 in 4 mM) containing diethylene triamine pentaacetic acid (DTPA) was added, and the yellow color of TNB was visible in the mixed samples. The absorbance was measured at 412 nm with a UV-vis spectrometer (UV2600, Shimadzu). The DTT, TCA, and DTNB were all dissolved in 0.1 M phosphate buffer (pH 7.4) containing 1 mM DTPA. and the corresponding filter blank was analyzed to correct the DTT activity of the sample fractions. The DTT

consumption rate after subtracting the field blank was determined using the absorbance and normalized by the particulate mass (DTT_m, pmol/min/μg) (Verma et al., 2012; Fan et al., 2018). In this study, 1.4-phenanthraquinone was used to conduct a positive control, of which the DTT consumption rate was 0.46±0.03 μM DTT/min (n=10). The rate was similar to those reported in the previous studies (Fan et al., 2018; Lin and Yu, 2019).

3. Results and discussion

3.1. Abundance of WSOC, HULIS-C, and MSOC in BB and CC smoke samples

Table 1 summarizes the abundance of BrC fractions, including WSOC, HULIS-C, and MSOC, in BB and CC smoke $PM_{2.5}$ samples. As shown in Table 1, the average contribution of WSOC to smoke $PM_{2.5}$ was 2.9%–12% and 2.3%–22% for BB and CC, respectively. These results were comparable to the results obtained for smoke samples from the combustion of cherry leaves (16%), gingko tree leaves (6.0%) (Park et al., 2013), corn straw (5.9%), pine branches (6.4%) (Fan et al., 2016), and residential coals (4%–11%) (Li et al., 2018) and in the ambient $PM_{2.5}$ from rural and urban sites (4–13%) (Matos et al., 2015; Qin et al., 2018; Wu et al., 2020). This suggests that both BB and CC can release substantial amounts of water-soluble BrC into atmospheric aerosols. As the hydrophobic fraction of WSOC, the carbon content of HULIS (HULIS-C) accounted for 1.0%–7.8% and 0.5%–10% of BB and CC smoke $PM_{2.5}$, respectively. These values are comparable to the results obtained for BB smoke (5.9%–15.2%) (Fan et al., 2018; Huo et al., 2018), CC smoke (1.9%–4.8%) (Li et al., 2018), and atmospheric aerosols in Beijing (4.8%–9.4%) (Li et al., 2019), with an average value of 7.2% ± 3.3%, therefore confirming the important contributions made by BB

271 and CC to atmospheric HULIS. As a comparison, the contribution of MSOC to smoke $PM_{2.5}$
272 was 6.4%–47% and 9.4%–73% for BB and CC, respectively, with both values being much
273 higher than the contributions of the water-soluble fractions (WSOC and HULIS-C) in the
274 same smoke samples. Similar results have been reported in previous studies (Li et al., 2018;
275 Cheng et al., 2016), which suggest that there are more organic compounds that could be
276 extracted by methanol than by water, and it could therefore be a better indicator of total BrC.
277 This result also indicated that BB and CC both released large amounts of water-insoluble BrC
278 compounds, including hydrophobic polycyclic aromatic hydrocarbons (PAHs) and
279 nitrogen/sulfur-containing heteroatomic PAHs (Geng et al., 2014; Dong et al., 2021; Huang et
280 al., 2020).

281 Some differences were observed among the different types of smoke samples. As shown
282 in Figure 1, the average contributions of the WSOC and HULIS-C fractions to the total
283 carbon (TC) were 22% ± 7.3% and 11% ± 3.8%, respectively, for BB smoke, which were
284 higher than the corresponding values of 19% ± 9.4% and 8.2% ± 4.0% for CC smoke. The
285 contribution of MSOC to OC was 69% ± 19% for BB, which was significantly lower than the
286 value of 97% ± 1.8% for CC. These results suggested that BB generally released the more
287 water-soluble OC fraction whereas more water-insoluble OC fraction was contained in the
288 smoke particles emitted from CC. These differences can be explained by the fact that biomass
289 fuels generally contain large amounts of biopolymers, such as carbohydrates (cellulose,
290 hemicellulose, etc.); the burning of biomass fuels produces more highly polar compounds,
291 such as phenols, polyols, and polysaccharides; and CC emits more relatively hydrophobic and
292 less polar components, such as coal tar and polycyclic aromatic species (Wu et al., 2014; Wu

et al., 2021; Huang et al., 2020).

3.2 Light absorption

AAE and MAE_{365} are important optical indicators of the light absorption properties of atmospheric BrC and were investigated for BB- and CC-derived BrC in this study. As shown in Figures 2a and c, the AAE values of the WSOC and HULIS-C fractions were 6.1–9.9 (mean 7.8 ± 1.6) and 7.2–9.6 (mean 8.5 ± 0.8), respectively, for BB smoke and 8.5–16 (mean 13 ± 2.9) and 10–16 (mean 14 ± 2.3), respectively, for CC smoke. These results were comparable to those measured for combustion-emitted aerosols with reported AAE values for HULIS of 7.4–8.3 (Park and Yu, 2016) and 6.2–8.1 (Fan et al., 2016, 2018) for BB smoke and 5.2–14 for CC smoke (Li et al., 2019). Moreover, the AAE values of BB WSOC and HULIS were also comparable to those reported for WSOC in urban aerosols in Beijing (mean 7.28 ± 0.24) (Cheng et al., 2016), HULIS in Amazon BB aerosols (~7.10) (Hoffer et al., 2006), urban aerosols in Beijing (5.3–5.8) (Yan et al., 2015), and aerosols in the Tibetan Plateau (7.14–9.35) (Wu et al., 2020) but higher than that (1.2–5.4, mean of 3.2) of water-soluble BrC in Los Angeles (Zhang et al., 2013). However, the AAE values of the water-soluble BrC fraction from CC were almost higher than those in ambient aerosols, as described above. The AAE values for MSOC were 5.62–6.95 for BB smoke and 8.46–10.0 for CC smoke. It was obvious that the AAE value of BB MSOC was comparable to that of urban aerosols (average 7.10 ± 0.45) in Beijing (Cheng et al., 2016) and the reported value (5.0–6.5) for urban aerosols in India (Mukherjee et al., 2020), but the AAE values of CC MSOC were likely higher than those for urban aerosols. It is obvious that CC-derived BrC

315 fractions (WSOC, HULIS-C, and MSOC) generally have relatively higher AAE values than
316 ambient BrC, thereby suggesting that the contribution of CC may improve the AAE values of
317 BrC in the atmosphere and should not be ignored.

318 As shown in Figures 2a and c, the average AAE values of the WSOC, HULIS-C, and
319 MSOC fractions in BB smoke were all lower than those for the same BrC fraction in CC
320 smoke, indicating that BB-derived BrC had a weaker wavelength dependence than
321 CC-derived BrC. This finding agreed with the results reported in a previous study (Fan et al.,
322 2016). The AAE values of the BrC fraction also varied according to the type of BrC fraction.
323 HULIS-C had the highest AAE values, which were slightly higher than those for WSOC but
324 much higher than those for MSOC (Figures 2a and 2c), indicating that water-soluble BrC
325 fractions had a greater wavelength dependency than the corresponding MSOC. This was
326 similar to the results of previous studies that found higher AAE values for WSOC than
327 MSOC in ambient aerosols (Cheng et al., 2016; Kim et al., 2016) and can be explained by the
328 fact that the strongly light-absorbing organic molecules are generally comprised of aromatic
329 structures with a high degree of conjugation and low solubility in water.

330 MAE_{365} is an important parameter that characterizes the light absorption ability of
331 atmospheric BrC. As shown in Figures 2b and d, the MAE_{365} values of WSOC and HULIS-C
332 were 0.9–1.5 (mean 1.2 ± 0.3) and 1.1–1.6 (mean 1.3 ± 0.2) m^2/gC, respectively, for BB
333 smoke and 0.2–0.8 (mean 0.3 ± 0.2) and 0.3–1.1 (mean 0.4 ± 0.3) m^2/gC, respectively, for CC
334 smoke. As the hydrophobic fraction of WSOC, the MAE_{365} values of HULIS-C in BB and
335 CC smoke were slightly higher than that of the corresponding WSOC, suggesting that
336 HULIS-C had a stronger light absorbing ability. Moreover, the MAE_{365} values of WSOC and

HULIS-C in BB smoke were comparable with the results of previous studies of the WSOC and HULIS-C fractions in combustion-released smokes and ambient aerosols. For example, the reported MAE_{365} values of WSOC and HULIS-C were 0.8–1.6 and 1.0–1.5 m^2/gC, respectively, in BB smoke $PM_{2.5}$ (Park and Yu, 2016; Huo et al., 2018); 0.3–1.0 and 0.5–1.4 m^2/gC, respectively, in CC smoke particles (Li et al., 2018); and 0.1–1.5 m^2/gC in ambient aerosols (Cheng et al., 2016; Yan et al., 2015; Zou et al., 2020). In contrast, the MAE_{365} values for MSOC were 1.9–2.7 m^2/gC for BB smoke and 1.0–2.7 m^2/gC for CC smoke, which were 1.3–8.5 times higher than the corresponding values for HULIS-C and WSOC and suggest that MSOC had the strongest light absorption capacity. The MAE_{365} values of BB and CC MSOC were comparable to the MAE_{365} values of urban aerosols in Beijing winter (average 1.45 ± 0.26 m^2/gC) (Yan et al., 2015) and the water-insoluble BrC (0.85–2.45 m^2/gC) in summer and winter ambient aerosols in Xi'an, Northwest China (Li et al., 2020b). However, the values were higher than the MAE_{365} value of aerosol MSOC in the Central Tibetan Plateau (0.27–0.86 m^2/gC) (Wu et al., 2020), which may be due to the relatively low combustion source contribution in this region.

As shown in Figures 2b and d, some differences were observed among the BrC fractions. WSOC, HULIS-C, and MSOC in BB smoke all had relatively higher MAE_{365} values than the same BrC fractions from CC, which suggested that BrC components emitted from BB had a relatively higher light absorption ability than those from CC and may therefore have a higher radiative force (Alexander et al., 2008). This finding is important for accurately assessing the climate effects of BrC from different combustion sources.

3.3. Spectral EEM features and identification of PARAFAC components

3.3.1. The EEM fluorescence properties

Fluorescence spectroscopy is a highly sensitive analytical technique for the identification of the sources and types of fluorophores in natural organic matter. In recent decades, fluorescence spectroscopy has been widely used to characterize the fluorophores of atmospheric BrC in field and laboratory studies (Chen et al., 2017; Chen et al., 2016; Qin et al., 2018; Fan et al., 2020). The typical EEM spectra of WSOC, HULIS-C, and MSOC fractions from BB and CC are shown in Figure S2. To avoid concentration effects, the fluorescence spectra were normalized by the OC content of WSOC, HULIS-C, and MSOC; and the specific fluorescence intensities (a.u. L/(gC)) are shown.

In general, the different regions in the fluorescence spectra can be associated with organic fractions with different chemical characteristics (Table S1) (Chen et al., 2003; Cui et al., 2016; Qin et al., 2018). As shown in Figure S2, the EEM spectra were divided into five regions: protein-like amino acid (I), protein-like UV region (II, peak T_1), fulvic-like (III), tryptophan-like or microbial byproducts (IV, peak T_2), and humic-like (V) fluorophores (Qin et al., 2018; Cui et al., 2016; Chen et al., 2016). It was observed that the WSOC and HULIS-C fractions exhibited two types of fluorescence peaks at $\lambda_{ex}/\lambda_{em} \approx$ (220–240)/(350–390) nm (peak T_1) and $\lambda_{ex}/\lambda_{em} \approx$ (260–300)/(240–380) nm (peak T_2) (as marked in Figure S2), which were mainly located in regions II and IV, respectively. These bands in the same range as peaks T_1 and T_2 have previously been identified in the EEM fluorescence spectra of water-soluble organic matter from rainwater/fog water (Santos et al., 2009; Santos et al., 2012) and $PM_{2.5}$ in an industrial city in Northwest China (Qin et al., 2018). As shown in

Figure S2, the fluorescence peaks T_1 and/or T_2 were the dominant peaks for WSOC and HULIS-C in BB- and CC-derived smoke samples, which were consistent with previous observations of the WSOC and HULIS-C fractions from BB (Huo et al., 2018; Fan et al., 2020). In general, peak T_1 mainly corresponded to the protein-like UV region, with a minor contribution from fulvic-like substances; whereas peak T_2 was assigned as tryptophan-like or microbial byproduct fluorophores. However, as reported in recent studies, non-nitrogen-containing species, such as naphthalene and phenol-derived compounds, may also contribute to the fluorophores with peak T_2 in atmospheric aerosols (Chen et al., 2017, 2020). In addition, the intensity of peak T_1 for BB- and CC-derived HULIS-C fractions was clearly stronger than the peak in ambient HULIS described in previous studies (Chen et al., 2017; Chen et al., 2016; Fan et al., 2020; Qin et al., 2018), indicating that these BB- and CC-derived HULIS-C might consist of more protein-like and/or aromatic amino acids than atmospheric HULIS. However, these protein-like fluorescence peaks were observed to gradually decrease during the aging process (e.g., hydroxyl radicals or ozone oxidation) in previous studies (Fan et al., 2019, 2020). This implied that most protein-like fluorophores in BB or CC BrC fractions may have high reactivity.

As shown in Figure S2, the EEM spectra of the three MSOC fractions from crop straw burning all had a strong fluorescence peak at long emission wavelengths (E_X = 205–280 nm, E_M = 360–380 nm), which were located in regions V and IV and were generally assigned to humic-like fluorophores (Qin et al., 2018) or less oxygenated humic-like species (Chen et al., 2017; Chen et al., 2016). This peak was very weak or unobservable in the EEM fluorescence spectra of the WSOC and HULIS-C fractions, suggesting that the higher intensity of the

fluorescence peak was mainly due to water-insoluble organic compounds with a high degree of conjugation and/or aromaticity. As shown in Figure S2, unlike the EEM spectra of crop straw MSOC, the EEM spectra of the three types of wood branches all displayed two obvious fluorescence peaks (e.g., peaks T_1 and T_2). These differences in the EEM spectra between crop straw and wood burning-derived MSOC might be attributed to their molecular differences, which should be investigated in future studies. The EEM spectra of the four bituminous coal smoke MSOC fractions displayed a similar fluorescence peak T_2 in the EEM spectra, but only a strong peak T_1 was observed in the anthracite coal smoke MSOC. These differences indicate that the fluorophores of MSOC were significantly influenced by the type of fuel.

3.3.2. Identification of PARAFAC components

PARAFAC analysis further determined the fluorescent components of the water-soluble BrC fraction (WSOC and HULIS-C) and MSOC. As shown in Figure 3a, WSOC and HULIS-C generally contained four types of fluorophores (C_W1–C_W4). Based on previous studies of BrC EEM in combustion aerosols and ambient aerosols (Chen et al., 2017; Chen et al., 2016; Huo et al., 2018; Qin et al., 2018), these four fluorophores could be assigned to two protein-like substances (C_W1 and C_W2), one polyphenol-like component (C_W3), and one humic-like compound (C_W4). The E_x/E_m maximum of C_W1 was located at 230/365 nm in region II and was confirmed to be protein-like UV fluorophores. C_W2 (E_X = 270 nm, E_M = 350 nm) was placed in region IV and was determined to be tryptophan-like or microbial byproduct compounds (Chen et al., 2016; Li et al., 2020a), which have been identified in

aerosol WSOM (Chen et al., 2016; Matos et al., 2015) and BB-derived primary and secondary WSOM (Huo et al., 2018). C_W3 (E_X = 205/275 nm, E_M = 330 nm) was located in regions I and IV and had the characteristics of aromatic protein-like fluorophores or polyphenol-like components, most likely representing the fluorescence properties of polyphenol-like components or compounds containing phenoxy groups (Mostofa et al., 2011). C_W4 (E_X = 215–320 nm, E_M = 415 nm) was located in the area where regions III and V overlap. These overlapping peaks were assigned to strong humic-like species fluorescence with an excitation wavelength = 245 nm and two weaker shoulder peaks (Chen et al., 2016; Li et al., 2020a; Qin et al., 2018; Huo et al., 2018; Fan et al., 2020); therefore, C_W4 was associated with typical humic-like fluorophores. In summary, the fluorescence components identified in the WSOC and HULIS-C fractions suggested that protein-like and humic-like substances were the two major backbone components in water-soluble BrC fractions.

As shown in Figure 3b, four independent fluorescence components were also identified by PARAFAC analysis of MSOC (C_M1–C_M4). These components were similar to those of WSOC and HULIS-C, especially the positioning of the main peaks of the four fluorescent fluorophores. However, some small differences for component 2 (C_W2 and C_M2) and component 4 (C_W4 and C_M4) fluorophores were also observed. Unlike C_W2 in WSOC and HULIS-C, C_M2 in MSOC had its Ex/Em maximum at 285/360 nm, which was assigned to tryptophan-like compounds (Fan et al., 2020; Qin et al., 2018). In addition, two lower intensities of peaks at a lower excitation wavelength were also detected. The position of this fluorescence was closer to that of the typical tryptophan-like chromophores in aquatic DOM (Murphy et al., 2010). C_M4 in MSOC had a strong peak (EX = 255 nm, EM = 295 nm) but

447 without the shoulder peaks observed for C_W4 in WSOC (Chen et al., 2016; Hou et al., 2018).

448 The relative contributions of individual chromophores identified by PARAFAC analysis
449 were calculated to express the relative contribution of each independent chromophore to the
450 overall fluorescence properties and are shown in Figure 4. The protein-like fluorescence
451 group (components 1 and 2), which were located at low emission wavelengths, dominated the
452 fluorophores of the BrC fractions in most BB and CC smoke samples. As shown in Figure 4,
453 the contributions of protein-like substances in WSOC, HULIS-C, and MSOC were 47%–80%,
454 44%–87%, and 42%–70% (except CS MSOC), respectively, which were higher than the
455 contributions of polyphenol-like or humic-like substances in the same BrC fraction. These
456 results are similar to the results reported for BrC from biomass combustion emissions in
457 previous studies (Huo et al., 2018; Fan et al., 2020). However, they were significantly
458 different from the EEM-PARAFAC properties of BrC in ambient aerosols, in which
459 component 4 was the most abundant chromophore (Chen et al., 2016; Li et al., 2020a).
460 However, component 4 accounted for only 13%–33% (except CS MSOC) and 3.8%–31% of
461 the BB and CC BrC fluorescence intensities, respectively, which were significantly lower
462 than those reported previously in ambient aerosols (30%–38%) (Li et al., 2020a). Moreover,
463 the contribution of polyphenol-like chromophores was 4.0%–39% and was comparable to
464 that of ambient aerosols (18%–26%) (Li et al., 2020a; Chen et al., 2016). It is obvious that the
465 four fluorescent components were all detected in the BrC fractions in combustion-derived
466 smokes and atmospheric aerosols; however, the protein-like compounds were the dominant
467 fluorophores in combustion-derived BrC whereas a relatively higher content of humic-like
468 fluorophores was identified in ambient aerosol BrC. These differences may be due to the

469 influence of various sources and atmospheric chemical processes on fluorophores (Li et al.,
470 2020a; Fan et al., 2020).

471 Furthermore, some differences were also observed among the BrC fractions derived
472 from different sources. As shown in Figure 4, the water-soluble BrC (WSOC and HULIS-C)
473 from wood burning had a relatively higher content of component 3 than the water-soluble
474 BrC from crop straw burning, which may be associated with the relatively large amount of
475 lignin components in wood materials. In addition, even though their maturity was very
476 different, there was no regular trend in the relative content of the fluorescent groups.

477

478 **3.4. ^{1}H-NMR spectroscopy**

479 ^{1}H-NMR is an important analytical tool for the investigation of the functional groups of
480 WSOC and HULIS in rural/urban aerosols (Fan et al., 2016; Zou et al., 2020) and rainwater
481 (Santos et al., 2009; Santos et al., 2012). The typical ^{1}H-NMR spectra of the WSOC,
482 HULIS-C, and MSOC fractions in smoke emitted from BB crop straw (e.g., WS) and CC
483 (e.g., B-1) are shown in Figure 5, and the ^{1}H-NMR spectra of other BB and CC BrC fractions
484 are shown in Figure S3. These BrC fractions had ^{1}H-NMR spectra similar to those derived
485 from atmospheric HULIS and/or WSOC in rainwater (Santos et al., 2009; Santos et al., 2012),
486 BB aerosols (Fan et al., 2016), and ambient aerosols in urban and rural regions (Zou et al.,
487 2020).

488 As shown in Figure 5, the ^{1}H-NMR spectra were mainly composed of several distinct
489 sharp peaks superimposed on an unresolved broad band. According to previous studies and
490 reference NMR spectra (Zou et al., 2020; Chalbot et al., 2014; Chalbot et al., 2016), these

sharp peaks can be ascribed to low molecular weight organic compounds, such as levoglucosan (δ3.52, δ3.67, δ4.08, and δ5.45 ppm), glucose (δ3.88–δ3.91 and δ3.81–δ3.85 ppm), and fructose (δ3.79–δ3.84 ppm) associated with BB emissions; phthalic acid (δ7.45–δ7.47 and δ7.58 ppm) and terephthalic acid (δ8.01 ppm) associated with anthropogenic activity; and the CH_3 in trimethylamine (δ2.71 and δ2.89 ppm), dimethylamine (δ2.72 ppm), and monomethylamine (δ2.55 ppm) coemitted with ammonia. The relatively few and/or weak sharp peaks in the ^{1}H-NMR spectra of HULIS-C compared with those of WSOC may be the result of low molecular weight organic compounds that have been removed from HULIS-C through SPE isolation. In addition, all BB-derived WSOC had a high intensity of sharp peaks associated with carbohydrates, such as levoglucosan, glucose, and fructose resonances, which may be released from the thermal reactions of biopolymers, such as celluloses. As a comparison, several peaks (δ0.90 and δ1.35 ppm) were observed in MSOC and were mainly located in the aliphatic region. These peaks were weaker in WSOC and HULIS-C, suggesting that more less polar aliphatic compounds were present in the MSOC fraction.

Despite some sharp peaks being identified, most of the signals in the ^{1}H-NMR spectra of the BrC fractions presented a continuous unresolved distribution, suggesting that BrC consists of a complex mixture of organic substances (Fan et al., 2016; Chalbot et al., 2014; Chalbot et al., 2016). As shown in Figure 5, the functional groups of smoke BrC could be divided into four representative categories: (1) R-H: aliphatic protons in alkyl chains (0.6–1.9 ppm), including methyl (R-CH_3) protons, methylene (R-CH_2) protons, and methyne (R-CH) protons; (2) H-C-C=: aliphatic protons bound to carbon atoms adjacent to unsaturated groups (1.9–3.2 ppm), including carbonyl (H-C-C=O) and imino (H-C-C=N) groups or aromatic

rings; (3) H-C-O: protons bound to oxygenated aliphatic carbons atoms in alcohols, polyols, ethers, and esters (3.4–4.4 ppm), generally indicating that carbohydrates and ethers were present in organic matter; and (4) Ar-H: protons bound to aromatic carbon atoms (6.5–8.5 ppm) (Fan et al., 2016; Zou et al., 2020). The distribution of the four types of protons was obtained by integrating the area of the observed ^{1}H-NMR bands for each sample and is shown in Table 2. These functional groups were also observed in the ^{1}H-NMR spectra of HULIS in ambient aerosols. In general, HULIS in ambient aerosols (Chalbot et al., 2014; Chalbot et al., 2016) and rainwater (Santos et al., 2012) were characterized by the predominance of H-C (41%–60%), moderate contents of H-C-C= (25%–34%) and H-C-O (4.0%–49%), and a lesser contribution of Ar-H (2.0%–6.0%). However, it was obvious that the relative content of Ar–H groups (18%–37%) in HULIS-C from both combustion processes (BB and CC) was higher than the levels in ambient HULIS (Table 2), which suggests that BB- and CC-derived HULIS-C contained more aromatic structures than ambient HULIS. This was consistent with reports that more aromatic structures are observed in HULIS in colder season aerosol particles in northern China, which may be related to the amount of residential coal and straw combustion (Li et al., 2018; Sun et al., 2017).

As shown in Table 2, the relative contents of the four functional groups (i.e., R-H, H-C-C=, H-C-O, and Ar-H) varied with the type of BrC. For example, BB WSOC was always characterized by a relatively high level of oxygenated H-C-O groups and a relatively low level of aliphatic R-H groups compared with the corresponding MSOC extracted with methanol. As shown in Figure 5, several strong signals in aliphatic R-H were also identified in MSOC, but they were weaker in the WSOC fraction. This was considered reasonable

because the less polar aliphatic compounds were difficult to dissolve in water but could be extracted by methanol. As the hydrophobic fraction of WSOC, HULIS-C contained a relatively higher content of the Ar-H group and a relatively lower content of the oxygenated H-C-O group than the original WSOC for all BB and CC smoke samples. This was due to most of the low molecular oxygenated compounds not being retained by the hydrophilic-lipophilic balance cartridges and the enrichment of aromatic species (Fan et al., 2016; Zou et al., 2020).

Some distinct differences in the distribution of functional groups were also observed among the BrC fractions from BB and CC. As shown in Figure 5, several oxygenated compounds (e.g., levoglucosan) were identified, with higher intensity signals in the BB WSOC fraction, but they were weaker in the WSOC fraction from CC. The relative content of the H-C-O group was in the range of 34%–54% for the six BB WSOCs, which was higher than the values (9.0–34%) for the five CC WSOCs. These oxygenated aliphatic compounds were mainly assigned to carbohydrates and polyols that may be caused by the degradation of biomass polymers such as cellulose (Fan et al., 2012; Fan et al., 2016; Lin et al., 2016). In contrast, the BrC fractions from CC indicated a relatively higher level of unsaturated functional groups (Table 2). For example, there was a relatively higher content of Ar–H (30%–37%) and H-C-C= (34%–40%) in the smoke HULIS-C from CC than from BB, indicating that CC HULIS-C contained more unsaturated structures, such as aromatic structures and unsaturated aliphatics (Wu et al., 2014; Dong et al., 2021; Huang et al., 2020).

3.5 Oxidative potential

557 The oxidative potential of the BB- and CC-derived BrC fractions (i.e., WSOC,
558 HULIS-C, and MSOC) was investigated through a DTT assay, and the results are shown in
559 Table S2 and Figure 6. The DTT_m value of WSOC ranged from 0.5 pmol/min/μg (B-3) to 7.4
560 pmol/min/μg (CS) with a mean of 3.8 pmol/min/μg. These DTT_m values are comparable with
561 those for the water soluble fractions of BB, CC, and diesel soot (1.4±0.6, 2.1±2.3 and 1.1±0.4
562 pmol/min/μg) (Li et al., 2019; Zhu et al., 2019) but were much lower than the ranges of 14–
563 25 pmol/min/μg in Los Angeles wildfire aerosol samples, 22−68 pmol/min/μg in Atlanta
564 $PM_{2.5}$ samples, and 0.13±0.10 nmol/min/μg in Beijing $PM_{2.5}$ samples (Verma et al., 2012;
565 Bates et al., 2019, Yu et al., 2019). These results suggested that the water-soluble fraction
566 from BB and CC in this study had a weaker ROS generation capacity than ambient aerosols,
567 which was likely due to the differences in the chemical composition of water-soluble
568 fractions in BB and CC smoke particles and ambient aerosols (Lin and Yu, 2011; Dou et al.,
569 2015; Wong et al., 2019; Lin and Yu, 2019). In general, ambient aerosols contain various
570 sources; and the contribution of other sources, such as vehicle emissions or anthropogenic
571 emissions, and transition metals (e.g., Fe, Cu) could increase the ability of atmospheric
572 water-soluble fractions to produce ROS species (Ma et al., 2018; Li et al., 2019). In addition,
573 because of the evaporative loss of non- or less-DTT active semivolatile organic compounds,
574 the DTT activities of BB-derived water-soluble fractions were enhanced during the aging
575 process (Wong et al., 2019).

576 The DTT_m values of BB- and CC-derived HULIS-C ranged from 0.5 pmol/min/μg (B-3)
577 to 5.5 pmol/min/μg (RS) with a mean of 2.3 pmol/min/μg. These values were lower than the
578 range (15–45 pmol/min/μg) previously reported for ambient HULIS measured with the same

579 DTT assay (Lin and Yu, 2011; Ma et al., 2018; Verma et al., 2012). As an important
580 component of WSOC, HULIS-C accounted for 63.1%±15.5% (41.4%–90.6%) of the DTT
581 activity in WSOC in the BB and CC samples. Moreover, these values were always higher
582 than the carbon proportions of HULIS-C/WSOC for the same sample (Table 1), therefore
583 indicating that hydrophobic HULIS-C was an important redox-active fraction in the BB- and
584 CC-derived WSOC compounds. This result was comparable with the higher oxidative
585 contribution (64%) of HULIS-C following water extracts from ambient aerosols in Atlanta
586 (Verma et al., 2012). This phenomenon can be explained by the specific organic species and
587 functional groups with DTT activity in HULIS-C. As described in previous studies and in this
588 study, the hydrophobic organic fractions isolated by the SPE column are mainly comprised of
589 aromatic compounds (Sannigrahi et al., 2006; Fan et al., 2016; Huo et al., 2018). These
590 compounds most likely include some of the redox-active species such as nitro-PAHs and
591 quinones (Verma et al., 2012), which can catalyze the oxidation of cellular antioxidants and
592 generate ROS species (Verma et al., 2012; Lin and Yu, 2011). In addition, as the charge
593 transfer intermediate, the reversible redox sites in HULIS lead to continuous ROS production
594 (Ma et al., 2018; Lin and Yu, 2011).

595 The DTT_m values of MSOC were in the range of 3.1 pmol/min/μg (B-4) to 84
596 pmol/min/μg (RS). These values were comparable to those reported in previous studies
597 involving atmospheric aerosol methanol extracts (~55 pmol/min/μg) (Verma et al., 2012). As
598 shown in Figure 6, the DTT_m values of MSOC were much higher than those of WSOC and
599 HULIS-C from the same smoke samples, which suggested that the water-insoluble
600 components possessed significant oxidative properties that are relevant in toxicological

studies (Verma et al., 2012). These results were consistent with the results of previous studies showing that water-insoluble compounds made the largest contribution to the oxidative potential (Verma et al., 2012; Verma et al., 2015).

The DTT_m values of the BrC fractions varied with the type of fuel. As shown in Table S2, the DTT_m values of BB WSOC were 4.5–7.4 pmol/min/μg, which was significantly higher than the range of 0.5–2.1 pmol/min/μg for CC WSOC. Similar results were also observed for the HULIS and MSOC fractions (Figure 6). These results indicated that the BrC fractions from BB had higher oxidative potential values than those from CC and therefore more readily catalyzed the generation of ROS. Furthermore, no regular variations were observed for the oxidative potential of water-soluble BrC (e.g., WSOC and HULIS-C) in BB or CC smoke samples, but the MSOC in crop straw smoke had a much higher DTT_{mass} value than the MSOC in smoke samples from wood burning and CC. These differences were associated with the differences in the amounts of redox-active compounds in each BrC fraction. There is a need for more studies to investigate the relationship between the molecular structures in BB smoke BrC and their DTT activities.

3.6 Correlation between oxidative potential and chemical compositions of BrCs

The BrCs produced by the BB and CC processes generally have different oxidative potentials. The oxidative potential values of water-soluble BrC (WSOC and HULIS-C) were much lower than those in MSOC, and the BB BrC fractions had higher oxidative potential values than CC BrC fractions. These results suggested that BrC from different sources exhibited distinct redox properties (Lin and Yu, 2011). To elucidate the association of

chemical characteristics with the oxidative potential of BB and CC, principal component analysis (PCA) and Pearson correlation coefficients were conducted. Because the optical and chemical properties were all obtained based on organic matter rather than PM, the oxidative potential value (DTT_c) corrected by the carbon mass of each fraction was used here to present DTT activities, as well as the capacity to produce ROS species. In addition, considering the statistical significance and quantity, the WSOC, HULIS-C and MSOC data were analyzed together.

The results are shown in Figure 7 and Table 3. It is obvious that DTT_c showed a positive loading for both principal component 1 (PC1) and principal component 2 (PC2), and DTT_c was grouped with fluorophores C4 and MAE_{365}. These results are also given by the Pearson correlation coefficient analysis in which the DTT_c values showed significant positive correlations with the parameters MAE_{365} ($R=0.697$, $p<0.01$) and C4 proportion ($R=0.560$, $p<0.01$). These results suggested that fluorophore C4 and high light-absorbing components may significantly contribute to the DDT activities of BrC compounds.

Moreover, a significant positive relationship was also observed for C4 and MAE_{365} ($R=0.531$, $p<0.01$), which indicated that C4 may be the main substance leading to the light absorption of BrC. As reported previously, MAE_{365} is related to the aromatic structure of the conjugated system (Andrade-Eiroa et al., 2013, Fan et al., 2018), and fluorophore C4 was considered to be a highly oxygenated species containing more carbonyl and carboxyl groups (Chen et al., 2016, Li et al., 2020a). Therefore, the C4 component may mainly comprise chemical species with a conjugated system and highly oxygenated species, such as quinones or aromatic acids, which were believed to be the key components for the enhancement of the

ability of BrC to produce ROS species (Lin and Yu, 2011, Jiang et al., 2016, Verma et al., 2012). These results also explained that the water-soluble BrC fractions in BB and CC smoke showed relatively lower DTT_m values than those in ambient aerosols, in which distinctly higher contents of fluorophore C4 were observed in the water-soluble fraction (Matos et al., 2015; Chen et al., 2016).

We note that a positive correlation was observed between DTT_c and R-H and a negative correlation was observed between DTT_c and Ar-H; however, it is scientifically unreasonable. The main reason is that ^1H NMR spectroscopy only measures the concentrations of nonexchangeable hydrogen functional groups in BrC compounds. Some organic compounds not carrying nonexchangeable hydrogen atoms, such as carbonyl or carboxylic groups in BrC, cannot be detected by ^1H NMR (Chalbot and Kavouras 2014; Paglione et al., 2014). However, some of these oxygenated functional groups likely have the ability to catalyze the generation of ROS species (Lin and Yu, 2011; Verma et al., 2015). In addition, the H/C ratios of different hydrogen functional groups (i.e., R-H, H-C-C=, H-C-O, and Ar-H) are very different; thus, the relative abundances of hydrogen functional groups are difficult to compare with the carbon functional groups in BrC compounds (Decesari et al., 2007). Therefore, it is necessary that other NMR techniques such as solution-state ^{13}C NMR and two-dimensional heteronuclear (^1H-^{13}C) NMR be used to explore the chemical functional groups associated with the oxidative potential of BrC in future studies.

4. Conclusions

In this study, the primary BrC fractions (i.e., WSOC, HULIS-C, and MSOC) emitted

667 from BB and CC were comprehensively investigated to determine their content, light
668 absorption, fluorophores, chemical properties, and oxidative potential. The results indicated
669 that both BB and CC were important sources of atmospheric BrC. It was found that BB
670 generated more of the water-soluble BrC fraction whereas CC released more of the
671 methanol-soluble BrC fraction in smoke $PM_{2.5}$. The results also enhanced our understanding
672 of the optical characteristics, chemical composition, and oxidative potential of the water- and
673 methanol-soluble BrC fractions. The MSOC fraction had higher MAE_{365} values than
674 HULIS-C and WSOC, suggesting that water-insoluble BrC possessed a stronger light
675 absorbing capacity. In addition, BB BrC generally had higher MAE_{365} and lower AAE values
676 than the corresponding CC BrC fractions, suggesting that the former had a higher light
677 absorption capacity and weaker wavelength dependence. The EEM-PARAFAC analysis
678 identified two protein-like compounds, one polyphenol-like component, and one humic-like
679 compound for all BrC fractions, among which the protein-like compounds were the dominant
680 components. The ^{1}H NMR analysis showed that the BB and CC BrC fractions contained R-H,
681 H-C-C=, H-C-O, and Ar-H groups, among which WSOC and HULIS-C were always
682 characterized by more oxygenated H-C-O groups and fewer aliphatic R-H groups than
683 MSOC. In addition, water-soluble BB BrC contained more highly oxygenated groups,
684 suggesting that they may have a stronger influence on the binding of metals by organic
685 aerosols. Our study also indicated that MSOC had higher DTT_m values than WSOC and
686 HULIS-C, suggesting a higher ROS generation capacity. The BB BrC fractions generally had
687 a higher oxidative potential than CC BrC, which may suggest that BB BrC was more readily
688 able to catalyze the generation of ROS and therefore lead to more severe harm to human

health. More importantly, the PCA and Pearson correlation analysis indicated that highly oxygenated humic-like fluorophore C4 may be an important DTT active substance in BrC.

It should be noted that the BB and CC BrC fractions would experience a series of chemical reactions once they are emitted into the atmosphere, resulting in changes to their optical properties and DTT activities. Thus, future studies should focus on the chemical, optical, and oxidative potential characteristics of BrC during the aging processes with smoke particles in the tropospheric environment (Fan et al., 2020; Wong et al., 2019).

Data availability. The research data can be accessed upon request to the corresponding author (songjzh@gig.ac.cn).

Author contributions. J. Song and P. Peng designed the research together. T. Cao, M. Li, and C. Zou conducted the combustion experiments. T. Cao, M. Li, and C Yu extracted and analyzed the BrC fractions. T. Cao and J. Song wrote the paper. X. Fan, J Wang, Z Yu, and P. Peng commented on and revised the paper.

Competing interests. The authors declare that they have no conflicts of interest.

Acknowledgments. This study was supported by the National Natural Science Foundation of China (41977188 and 41673177), the State Key Laboratory of Organic Geochemistry, GIGCAS (SKLOG2020-3), and Guangdong Foundation for Program of Science and Technology Research (2019B121205006). We greatly appreciate the assistance of two

anonymous reviewers for the helpful comments that greatly improved the quality of this manuscript.

References

Alexander, D. T. L., Crozier, P. A., and Anderson, J. R.: Brown carbon spheres in East Asian outflow and their optical properties, Science, 321, 833-836, 10.1126/science.1155296, 2008.

Andrade-Eiroa, Á., Canle, M., and Cerdá, V.: Environmental Applications of Excitation-Emission Spectrofluorimetry: An In-Depth Review I, Applied Spectroscopy Reviews, 48, 1-49, 10.1080/05704928.2012.692104, 2013.

Andreae, M. O., and Gelencser, A.: Black carbon or brown carbon? The nature of light-absorbing carbonaceous aerosols, Atmospheric Chemistry and Physics, 6, 3131-3148, DOI 10.5194/acp-6-3131-2006, 2006.

Atwi, K., Mondal, A., Pant, J., Cheng, Z., El Hajj, O., Ijeli, I., Handa, H., and Saleh, R.: Physicochemical properties and cytotoxicity of brown carbon produced under different combustion conditions, Atmospheric Environment, 244, 117881, 10.1016/j.atmosenv.2020.117881, 2021.

Bai, Z., Zhang, L., Cheng, Y., Zhang, W., Mao, J., Chen, H., Li, L., Wang, L., and Chen, J.: Water/Methanol-Insoluble Brown Carbon Can Dominate Aerosol-Enhanced Light Absorption in Port Cities, Environmental science & technology, 54, 14889-14898, 10.1021/acs.est.0c03844, 2020.

733 Bates, J. T., Fang, T., Verma, V., Zeng, L., Weber, R. J., Tolbert, P. E., Abrams, J. Y., Sarnat, S.
734 E., Klein, M., Mulholland, J. A., and Russell, A. G.: Review of Acellular Assays of
735 Ambient Particulate Matter Oxidative Potential: Methods and Relationships with
736 Composition, Sources, and Health Effects, Environmental science & technology, 53,
737 4003-4019, 10.1021/acs.est.8b03430, 2019.
738 Chalbot, M. G., Brown, J., Chitranshi, P., da Costa, G. G., Pollock, E. D., and Kavouras, I. G.:
739 Functional characterization of the water-soluble organic carbon of size-fractionated
740 aerosol in the southern Mississippi Valley, Atmos Chem Phys, 14, 6075-6088,
741 10.5194/acp-14-6075-2014, 2014.
742 Chalbot, M. C., and Kavouras, I. G.: Nuclear magnetic resonance spectroscopy for
743 determining the functional content of organic aerosols: a review, Environmental
744 pollution, 191, 232-249, 10.1016/j.envpol.2014.04.034, 2014.
745 Chalbot, M. G., Chitranshi, P., da Costa, G. G., Pollock, E., and Kavouras, I. G.:
746 Characterization of water-soluble organic matter in urban aerosol by (1)H-NMR
747 spectroscopy, Atmos Environ (1994), 128, 235-245, 10.1016/j.atmosenv.2015.12.067,
748 2016.
749 Chen, Q., Miyazaki, Y., Kawamura, K., Matsumoto, K., Coburn, S., Volkamer, R., Iwamoto,
750 Y., Kagami, S., Deng, Y., Ogawa, S., Ramasamy, S., Kato, S., Ida, A., Kajii, Y., and
751 Mochida, M.: Characterization of Chromophoric Water-Soluble Organic Matter in
752 Urban, Forest, and Marine Aerosols by HR-ToF-AMS Analysis and Excitation-Emission
753 Matrix Spectroscopy, Environmental science & technology, 50, 10351-10360,
754 10.1021/acs.est.6b01643, 2016.

Chen, Q., Ikemori, F., Nakamura, Y., Vodicka, P., Kawamura, K., and Mochida, M.: Structural and Light-Absorption Characteristics of Complex Water-Insoluble Organic Mixtures in Urban Submicrometer Aerosols, Environmental science & technology, 51, 8293-8303, 10.1021/acs.est.7b01630, 2017.

Chen, Q., Wang, M., Wang, Y., Zhang, L., Li, Y., and Han, Y.: Oxidative Potential of Water-Soluble Matter Associated with Chromophoric Substances in PM2.5 over Xi'an, China, Environmental science & technology, 53, 8574-8584, 10.1021/acs.est.9b01976, 2019.

Chen, Q., Li, J., Hua, X., Jiang, X., Mu, Z., Wang, M., Wang, J., Shan, M., Yang, X., Fan, X., Song, J., Wang, Y., Guan, D., and Du, L.: Identification of species and sources of atmospheric chromophores by fluorescence excitation-emission matrix with parallel factor analysis, The Science of the total environment, 718, 137322, 10.1016/j.scitotenv.2020.137322, 2020.

Chen, W., Westerhoff, P., Leenheer, J. A., and Booksh, K.: Fluorescence excitation - Emission matrix regional integration to quantify spectra for dissolved organic matter, Environmental science & technology, 37, 5701-5710, 10.1021/es034354c, 2003.

Chen, Y., and Bond, T. C.: Light absorption by organic carbon from wood combustion, Atmospheric Chemistry and Physics, 10, 1773-1787, DOI 10.5194/acp-10-1773-2010, 2010.

Cheng, Y., He, K. B., Du, Z. Y., Engling, G., Liu, J. M., Ma, Y. L., Zheng, M., and Weber, R. J.: The characteristics of brown carbon aerosol during winter in Beijing, Atmospheric Environment, 127, 355-364, 10.1016/j.atmosenv.2015.12.035, 2016.

Cui, X., Zhou, D., Fan, W., Huo, M., Crittenden, J. C., Yu, Z., Ju, P., and Wang, Y.: The effectiveness of coagulation for water reclamation from a wastewater treatment plant that has a long hydraulic and sludge retention times: A case study, Chemosphere, 157, 224-231, 10.1016/j.chemosphere.2016.05.009, 2016.

Decesari, S., Mircea, M., Cavalli, F., Fuzzi, S., Moretti, F., Tagliavini, E., and Facchini, M. C.: Source attribution of water-soluble organic aerosol by nuclear magnetic resonance spectroscopy, Environmental science & technology, 41, 2479-2484, 10.1021/es0617111, 2007.

Dong, Z., Jiang, N., Zhang, R., Xu, Q., Ying, Q., Li, Q., and Li, S.: Molecular characteristics, source contributions, and exposure risks of polycyclic aromatic hydrocarbons in the core city of Central Plains Economic Region, China: Insights from the variation of haze levels, The Science of the total environment, 757, 143885, 10.1016/j.scitotenv.2020.143885, 2021.

Dou, J., Lin, P., Kuang, B. Y., and Yu, J. Z.: Reactive Oxygen Species Production Mediated by Humic-like Substances in Atmospheric Aerosols: Enhancement Effects by Pyridine, Imidazole, and Their Derivatives, Environmental science & technology, 49, 6457-6465, 10.1021/es5059378, 2015.

Evangeliou, N., Kylling, A., Eckhardt, S., Myroniuk, V., Stebel, K., Paugam, R., Zibtsev, S., and Stohl, A.: Open fires in Greenland in summer 2017: transport, deposition and radiative effects of BC, OC and BrC emissions, Atmospheric Chemistry and Physics, 19, 1393-1411, 10.5194/acp-19-1393-2019, 2019.

Fan, X., Li, M., Cao, T., Cheng, C., Li, F., Xie, Y., Wei, S., Song, J., and Peng, P. a.: Optical

properties and oxidative potential of water-and alkaline-soluble brown carbon in smoke particles emitted from laboratory simulated biomass burning, Atmospheric Environment, 194, 48-57, 10.1016/j.atmosenv.2018.09.025, 2018.

Fan, X., Yu, X., Wang, Y., Xiao, X., Li, F., Xie, Y., Wei, S., Song, J., and Peng, P. a.: The aging behaviors of chromophoric biomass burning brown carbon during dark aqueous hydroxyl radical oxidation processes in laboratory studies, Atmospheric Environment, 205, 9-18, 10.1016/j.atmosenv.2019.02.039, 2019.

Fan, X., Cao, T., Yu, X., Wang, Y., Xiao, X., Li, F., Xie, Y., Ji, W., Song, J., Peng, P., amp, apos, and an: The evolutionary behavior of chromophoric brown carbon during ozone aging of fine particles from biomass burning, Atmospheric Chemistry and Physics, 20, 4593-4605, 10.5194/acp-20-4593-2020, 2020.

Fan, X. J., Song, J. Z., and Peng, P. A.: Comparison of isolation and quantification methods to measure humic-like substances (HULIS) in atmospheric particles, Atmospheric Environment, 60, 366-374, 10.1016/j.atmosenv.2012.06.063, 2012.

Fan, X. J., Wei, S. Y., Zhu, M. B., Song, J. Z., and Peng, P. A.: Comprehensive characterization of humic-like substances in smoke PM2.5 emitted from the combustion of biomass materials and fossil fuels, Atmospheric Chemistry and Physics, 16, 13321-13340, 10.5194/acp-16-13321-2016, 2016.

Gao, D., Mulholland, J. A., Russell, A. G., and Weber, R. J.: Characterization of water-insoluble oxidative potential of PM2.5 using the dithiothreitol assay, Atmospheric Environment, 224, 117327, 10.1016/j.atmosenv.2020.117327, 2020.

Geng, C., Chen, J., Yang, X., Ren, L., Yin, B., Liu, X., and Bai, Z.: Emission factors of

polycyclic aromatic hydrocarbons from domestic coal combustion in China, Journal of environmental sciences, 26, 160-166, 10.1016/s1001-0742(13)60393-9, 2014.

He, W., and Hur, J.: Conservative behavior of fluorescence EEM-PARAFAC components in resin fractionation processes and its applicability for characterizing dissolved organic matter, Water research, 83, 217-226, 10.1016/j.watres.2015.06.044, 2015.

Hoffer, A., Gelencser, A., Guyon, P., Kiss, G., Schmid, O., Frank, G. P., Artaxo, P., and Andreae, M. O.: Optical properties of humic-like substances (HULIS) in biomass-burning aerosols, Atmospheric Chemistry and Physics, 6, 3563-3570, DOI 10.5194/acp-6-3563-2006, 2006.

Hou, C., Shao, L., Hu, W., Zhang, D., Zhao, C., Xing, J., Huang, X., and Hu, M.: Characteristics and aging of traffic-derived particles in a highway tunnel at a coastal city in southern China, The Science of the total environment, 619-620, 1385-1393, 10.1016/j.scitotenv.2017.11.165, 2018.

Huang, R. J., Yang, L., Shen, J., Yuan, W., Gong, Y., Guo, J., Cao, W., Duan, J., Ni, H., Zhu, C., Dai, W., Li, Y., Chen, Y., Chen, Q., Wu, Y., Zhang, R., Dusek, U., O'Dowd, C., and Hoffmann, T.: Water-Insoluble Organics Dominate Brown Carbon in Wintertime Urban Aerosol of China: Chemical Characteristics and Optical Properties, Environmental science & technology, 54, 7836-7847, 10.1021/acs.est.0c01149, 2020.

Huo, Y. Q., Li, M., Jiang, M. H., and Qi, W. M.: Light absorption properties of HULIS in primary particulate matter produced by crop straw combustion under different moisture contents and stacking modes, Atmospheric Environment, 191, 490-499, 10.1016/j.atmosenv.2018.08.038, 2018.

Izhar, S., Gupta, T., and Panday, A. K.: Improved method to apportion optical absorption by black and brown carbon under the influence of haze and fog at Lumbini, Nepal, on the Indo-Gangetic Plains, Environmental pollution, 263, 114640, 10.1016/j.envpol.2020.114640, 2020.

Jiang, H., Jang, M., Sabo-Attwood, T., and Robinson, S. E.: Oxidative potential of secondary organic aerosols produced from photooxidation of different hydrocarbons using outdoor chamber under ambient sunlight, Atmospheric Environment, 131, 382-389, 10.1016/j.atmosenv.2016.02.016, 2016.

Kim, H., Kim, J. Y., Jin, H. C., Lee, J. Y., and Lee, S. P.: Seasonal variations in the light-absorbing properties of water-soluble and insoluble organic aerosols in Seoul, Korea, Atmospheric Environment, 129, 234-242, 10.1016/j.atmosenv.2016.01.042, 2016.

Kramer, A. J., Rattanavaraha, W., Zhang, Z., Gold, A., Surratt, J. D., and Lin, Y.-H.: Assessing the oxidative potential of isoprene-derived epoxides and secondary organic aerosol, Atmospheric Environment, 130, 211-218, 10.1016/j.atmosenv.2015.10.018, 2016.

Kumar, N. K., Corbin, J. C., Bruns, E. A., Massabo, D., Slowik, J. G., Drinovec, L., Mocnik, G., Prati, P., Vlachou, A., Baltensperger, U., Gysel, M., El-Haddad, I., and Prevot, A. S. H.: Production of particulate brown carbon during atmospheric aging of residential wood-burning emissions, Atmospheric Chemistry and Physics, 18, 17843-17861, 10.5194/acp-18-17843-2018, 2018a.

Kumar, V., Rajput, P., and Goel, A.: Atmospheric abundance of HULIS during wintertime in

865 Indo-Gangetic Plain: impact of biomass burning emissions, Journal of Atmospheric
866 Chemistry, 75, 385-398, 10.1007/s10874-018-9381-4, 2018b.
867 Laskin, A., Laskin, J., and Nizkorodov, S. A.: Chemistry of atmospheric brown carbon,
868 Chemical reviews, 115, 4335-4382, 10.1021/cr5006167, 2015.
869 Lawaetz, A. J., and Stedmon, C. A.: Fluorescence Intensity Calibration Using the Raman
870 Scatter Peak of Water, Applied Spectroscopy, 63, 936-940,
871 10.1366/000370209788964548, 2009.
872 Li, J., Chen, Q., Hua, X., Chang, T., and Wang, Y.: Occurrence and sources of chromophoric
873 organic carbon in fine particulate matter over Xi'an, China, The Science of the total
874 environment, 725, 138290, 10.1016/j.scitotenv.2020.138290, 2020a.
875 Li, J., Zhang, Q., Wang, G., Li, J., Wu, C., Liu, L., Wang, J., Jiang, W., Li, L., Ho, K. F., and
876 Cao, J.: Optical properties and molecular compositions of water-soluble and
877 water-insoluble brown carbon (BrC) aerosols in northwest China, Atmospheric
878 Chemistry and Physics, 20, 4889-4904, 10.5194/acp-20-4889-2020, 2020b.
879 Li, M., Fan, X., Zhu, M., Zou, C., Song, J., Wei, S., Jia, W., and Peng, P.: Abundances and
880 light absorption properties of brown carbon emitted from residential coal combustion in
881 China, Environmental science & technology, 10.1021/acs.est.8b05630, 2019.
882 Li, R., Han, Y., Wang, L., Shang, Y., and Chen, Y.: Differences in oxidative potential of black
883 carbon from three combustion emission sources in China, Journal of environmental
884 management, 240, 57-65, 10.1016/j.jenvman.2019.03.070, 2019.
885 Li, X., Han, J., Hopke, P. K., Hu, J., Shu, Q., Chang, Q., and Ying, Q.: Quantifying primary
886 and secondary humic-like substances in urban aerosol based on emission source

887 characterization and a source-oriented air quality model, Atmospheric Chemistry and
888 Physics, 19, 2327-2341, 10.5194/acp-19-2327-2019, 2019.
889 Lin, M., and Yu, J. Z.: Dithiothreitol (DTT) concentration effect and its implications on the
890 applicability of DTT assay to evaluate the oxidative potential of atmospheric aerosol
891 samples, Environmental pollution, 251, 938-944, 10.1016/j.envpol.2019.05.074, 2019.
892 Lin, P., and Yu, J. Z.: Generation of reactive oxygen species mediated by humic-like
893 substances in atmospheric aerosols, Environmental science & technology, 45,
894 10362-10368, 10.1021/es2028229, 2011.
895 Lin, P., Laskin, J., Nizkorodov, S. A., and Laskin, A.: Revealing Brown Carbon
896 Chromophores Produced in Reactions of Methylglyoxal with Ammonium Sulfate,
897 Environmental science & technology, 49, 14257-14266, 10.1021/acs.est.5b03608, 2015.
898 Lin, P., Aiona, P. K., Li, Y., Shiraiwa, M., Laskin, J., Nizkorodov, S. A., and Laskin, A.:
899 Molecular Characterization of Brown Carbon in Biomass Burning Aerosol Particles,
900 Environmental science & technology, 50, 11815-11824, 10.1021/acs.est.6b03024, 2016.
901 Ma, Y., Cheng, Y., Qiu, X., Cao, G., Fang, Y., Wang, J., Zhu, T., Yu, J., and Hu, D.: Sources
902 and oxidative potential of water-soluble humic-like substances ($HULIS_{WS}$) in fine
903 particulate matter ($PM_{2.5}$) in Beijing, Atmospheric Chemistry and Physics, 18,
904 5607-5617, 10.5194/acp-18-5607-2018, 2018.
905 Matos, J. T. V., Freire, S. M. S. C., Duarte, R. M. B. O., and Duarte, A. C.: Natural organic
906 matter in urban aerosols: Comparison between water and alkaline soluble components
907 using excitation-emission matrix fluorescence spectroscopy and multiway data analysis,
908 Atmospheric Environment, 102, 1-10, 10.1016/j.atmosenv.2014.11.042, 2015.

909 Mostofa, K. M. G., Wu, F. C., Liu, C. Q., Vione, D., Yoshioka, T., Sakugawa, H., and Tanoue,
910 E.: Photochemical, microbial and metal complexation behavior of fluorescent dissolved
911 organic matter in the aquatic environments, Geochem. J., 45, 235-254, 2011.
912 Moufarrej, L., Courcot, D., and Ledoux, F.: Assessment of the PM2.5 oxidative potential in a
913 coastal industrial city in Northern France: Relationships with chemical composition,
914 local emissions and long range sources, The Science of the total environment, 748,
915 141448, 10.1016/j.scitotenv.2020.141448, 2020.
916 Mukherjee, A., Dey, S., Rana, A., Jia, S., Banerjee, S., and Sarkar, S.: Sources and
917 atmospheric processing of brown carbon and HULIS in the Indo-Gangetic Plain:
918 Insights from compositional analysis, Environmental pollution, 267, 115440,
919 10.1016/j.envpol.2020.115440, 2020.
920 Murphy, K. R., Butler, K. D., Spencer, R. G. M., Stedmon, C. A., Boehme, J. R., and Aiken,
921 G. R.: Measurement of Dissolved Organic Matter Fluorescence in Aquatic Environments:
922 An Interlaboratory Comparison, Environmental science & technology, 44, 9405-9412,
923 10.1021/es102362t, 2010.
924 Murphy, K. R., Hambly, A., Singh, S., Henderson, R. K., Baker, A., Stuetz, R., and Khan, S.
925 J.: Organic matter fluorescence in municipal water recycling schemes: toward a unified
926 PARAFAC model, Environmental science & technology, 45, 2909-2916,
927 10.1021/es103015e, 2011.
928 Murphy, K. R., Stedmon, C. A., Graeber, D., and Bro, R.: Fluorescence spectroscopy and
929 multi-way techniques. PARAFAC, Analytical Methods, 5, 6557, 10.1039/c3ay41160e,
930 2013.

931 Nozière, B., González, N. J. D., Borg-Karlson, A.-K., Pei, Y., Redeby, J. P., Krejci, R.,
932 Dommen, J., Prevot, A. S. H., and Anthonsen, T.: Atmospheric chemistry in stereo: A
933 new look at secondary organic aerosols from isoprene, Geophysical Research Letters, 38,
934 n/a-n/a, 10.1029/2011gl047323, 2011.
935 Paglione, M., Saarikoski, S., Carbone, S., Hillamo, R., Facchini, M. C., Finessi, E.,
936 Giulianelli, L., Carbone, C., Fuzzi, S., Moretti, F., Tagliavini, E., Swietlicki, E., Eriksson
937 Stenström, K., Prévôt, A. S. H., Massoli, P., Canaragatna, M., Worsnop, D., and Decesari,
938 S.: Primary and secondary biomass burning aerosols determined by proton nuclear
939 magnetic resonance (¹H-NMR) spectroscopy during the 2008
940 EUCAARI campaign in the Po Valley (Italy), Atmospheric Chemistry and Physics, 14,
941 5089-5110, 10.5194/acp-14-5089-2014, 2014.
942 Park, S.-S., Sim, S. Y., Bae, M.-S., and Schauer, J. J.: Size distribution of water-soluble
943 components in particulate matter emitted from biomass burning, Atmospheric
944 Environment, 73, 62-72, 10.1016/j.atmosenv.2013.03.025, 2013.
945 Park, S. S., and Yu, J.: Chemical and light absorption properties of humic-like substances
946 from biomass burning emissions under controlled combustion experiments, Atmospheric
947 Environment, 136, 114-122, 10.1016/j.atmosenv.2016.04.022, 2016.
948 Qin, J., Zhang, L., Zhou, X., Duan, J., Mu, S., Xiao, K., Hu, J., and Tan, J.: Fluorescence
949 fingerprinting properties for exploring water-soluble organic compounds in PM 2.5 in an
950 industrial city of northwest China, Atmospheric Environment, 184, 203-211,
951 10.1016/j.atmosenv.2018.04.049, 2018.
952 Sannigrahi, P., Sullivan, A. P., Weber, R. J., and Ingall, E. D.: Characterization of

953 water-soluble organic carbon in urban atmospheric aerosols using solid-state C-13 NMR
954 spectroscopy, Environmental science & technology, 40, 666-672, 10.1021/es051150i,
955 2006.
956 Santos, P. S., Otero, M., Duarte, R. M., and Duarte, A. C.: Spectroscopic characterization of
957 dissolved organic matter isolated from rainwater, Chemosphere, 74, 1053-1061,
958 10.1016/j.chemosphere.2008.10.061, 2009.
959 Santos, P. S., Santos, E. B., and Duarte, A. C.: First spectroscopic study on the structural
960 features of dissolved organic matter isolated from rainwater in different seasons, The
961 Science of the total environment, 426, 172-179, 10.1016/j.scitotenv.2012.03.023, 2012.
962 Shen, G., Chen, Y., Wei, S., Fu, X., Zhu, Y., and Tao, S.: Mass absorption efficiency of
963 elemental carbon for source samples from residential biomass and coal combustions,
964 Atmospheric Environment, 79, 79-84, 10.1016/j.atmosenv.2013.05.082, 2013.
965 Singh, G. K., Choudhary, V., Rajeev, P., Paul, D., and Gupta, T.: Understanding the origin of
966 carbonaceous aerosols during periods of extensive biomass burning in northern India,
967 Environmental pollution, 270, 116082, 10.1016/j.envpol.2020.116082, 2021.
968 Sun, J., Zhi, G., Hitzenberger, R., Chen, Y., Tian, C., Zhang, Y., Feng, Y., Cheng, M., Zhang,
969 Y., Cai, J., Chen, F., Qiu, Y., Jiang, Z., Li, J., Zhang, G., and Mo, Y.: Emission factors
970 and light absorption properties of brown carbon from household coal combustion in
971 China, Atmospheric Chemistry and Physics, 17, 4769-4780, 10.5194/acp-17-4769-2017,
972 2017.
973 van der Werf, G. R., Randerson, J. T., Giglio, L., Collatz, G. J., Mu, M., Kasibhatla, P. S.,
974 Morton, D. C., DeFries, R. S., Jin, Y., and van Leeuwen, T. T.: Global fire emissions and

975 the contribution of deforestation, savanna, forest, agricultural, and peat fires
976 (1997-2009), Atmospheric Chemistry and Physics, 10, 11707-11735,
977 10.5194/acp-10-11707-2010, 2010.
978 Verma, V., Rico-Martinez, R., Kotra, N., King, L., Liu, J., Snell, T. W., and Weber, R. J.:
979 Contribution of water-soluble and insoluble components and their
980 hydrophobic/hydrophilic subfractions to the reactive oxygen species-generating
981 potential of fine ambient aerosols, Environmental science & technology, 46,
982 11384-11392, 10.1021/es302484r, 2012.
983 Verma, V., Fang, T., Guo, H., King, L., Bates, J. T., Peltier, R. E., Edgerton, E., Russell, A. G.,
984 and Weber, R. J.: Reactive oxygen species associated with water-soluble
985 PM_{2.5} in the southeastern United States: spatiotemporal trends
986 and source apportionment, Atmospheric Chemistry and Physics, 14, 12915-12930,
987 10.5194/acp-14-12915-2014, 2014.
988 Verma, V., Wang, Y., El-Afifi, R., Fang, T., Rowland, J., Russell, A. G., and Weber, R. J.:
989 Fractionating ambient humic-like substances (HULIS) for their reactive oxygen species
990 activity – Assessing the importance of quinones and atmospheric aging, Atmospheric
991 Environment, 120, 351-359, 10.1016/j.atmosenv.2015.09.010, 2015.
992 Wong, J. P. S., Tsagkaraki, M., Tsiodra, I., Mihalopoulos, N., Violaki, K., Kanakidou, M.,
993 Sciare, J., Nenes, A., and Weber, R. J.: Effects of Atmospheric Processing on the
994 Oxidative Potential of Biomass Burning Organic Aerosols, Environmental science &
995 technology, 53, 6747-6756, 10.1021/acs.est.9b01034, 2019.
996 Wu, D., Wang, Z., Chen, J., Kong, S., Fu, X., Deng, H., Shao, G., and Wu, G.: Polycyclic

997 aromatic hydrocarbons (PAHs) in atmospheric PM2.5 and PM10 at a coal-based
998 industrial city: Implication for PAH control at industrial agglomeration regions, China,
999 Atmospheric Research, 149, 217-229, 10.1016/j.atmosres.2014.06.012, 2014.
1000 Wu, G., Wan, X., Ram, K., Li, P., Liu, B., Yin, Y., Fu, P., Loewen, M., Gao, S., Kang, S.,
1001 Kawamura, K., Wang, Y., and Cong, Z.: Light absorption, fluorescence properties and
1002 sources of brown carbon aerosols in the Southeast Tibetan Plateau, Environmental
1003 pollution, 257, 113616, 10.1016/j.envpol.2019.113616, 2020.
1004 Wu, X., Liu, W., Gao, H., Alfaro, D., Sun, S., Lei, R., Jia, T., and Zheng, M.: Coordinated
1005 effects of air pollution control devices on PAH emissions in coal-fired power plants and
1006 industrial boilers, The Science of the total environment, 756, 144063,
1007 10.1016/j.scitotenv.2020.144063, 2021.
1008 Yan, C., Zheng, M., Sullivan, A. P., Bosch, C., Desyaterik, Y., Andersson, A., Li, X., Guo, X.,
1009 Zhou, T., Gustafsson, Ö., and Collett, J. L.: Chemical characteristics and light-absorbing
1010 property of water-soluble organic carbon in Beijing: Biomass burning contributions,
1011 Atmospheric Environment, 121, 4-12, 10.1016/j.atmosenv.2015.05.005, 2015.
1012 Yu, S., Liu, W., Xu, Y., Yi, K., Zhou, M., Tao, S., and Liu, W.: Characteristics and oxidative
1013 potential of atmospheric PM2.5 in Beijing: Source apportionment and seasonal variation,
1014 The Science of the total environment, 650, 277-287, 10.1016/j.scitotenv.2018.09.021,
1015 2019.
1016 Zhang, X., Lin, Y. H., Surratt, J. D., and Weber, R. J.: Sources, composition and absorption
1017 Angstrom exponent of light-absorbing organic components in aerosol extracts from the
1018 Los Angeles Basin, Environmental science & technology, 47, 3685-3693,

10.1021/es305047b, 2013.

Zhu, J., Chen, Y., Shang, J., and Zhu, T.: Effects of air/fuel ratio and ozone aging on physicochemical properties and oxidative potential of soot particles, Chemosphere, 220, 883-891, 10.1016/j.chemosphere.2018.12.107, 2019.

Zou, C., Li, M., Cao, T., Zhu, M., Fan, X., Peng, S., Song, J., Jiang, B., Jia, W., Yu, C., Song, H., Yu, Z., Li, J., Zhang, G., and Peng, P. a.: Comparison of solid phase extraction methods for the measurement of humic-like substances (HULIS) in atmospheric particles, Atmospheric Environment, 225, 117370, 10.1016/j.atmosenv.2020.117370, 2020.

Table 1. The contributions of BrC fraction (WSOC, HULIS, and MSOC) in smoke samples (%).

	Biomass burning						Coal combustion				
Contents (%)	WS	RS	CS	PW	CR	WP	B-1	B-2	B-3	B-4	AN
OC	44±5.6	41±12	24±6.4	19±3.8	26±8.7	23±13	61±5.4	64±11	68±7.6	69±6.9	9.5±5.0
EC	2.5±0.9	1.3±0.6	4.4±2.8	10±3.4	5.0±3.3	13±7.6	0.2±0.1	1.1±0.8	0.3±0.1	0.8±0.6	0.1±0.0
TC[a]	46±5.5	42±12	28±8.2	29±4.0	32±9.6	36±19	61±5.4	65±11	69±6.7	69±6.8	9.5±5.0
WSOC/PM[b]	11±2.7	12±1.6	9.7±0.2	3.9±1.1	7.6±0.3	2.9±0.7	15±0.4	22±4.1	9.2±1.5	4.7±0.4	2.3±1.1
HULIS-C/PM[b]	6.7±1.3	7.8±0.2	4.0±0.5	1.7±0.3	3.1±0.6	1.0±0.4	6.0±0.6	10±0.8	4.2±0.4	2.0±0.2	0.5±0.1
MSOC/PM[b]	40±0.9	47±0.8	20±1.4	12±1.2	15±0.9	6.4±0.7	57±5.4	73±2.9	65±6.8	71±0.7	9.4±5.7
WSOC/TC[c]	22±6.0	23±3.0	25±3.0	14±3.1	32±3.0	21±9.4	25±2.9	29±4.3	14±3.2	6.4±0.5	22±8.5
HULIS-C/TC[c]	14±2.8	14±0.4	11±2.7	5.9±0.8	13±1.6	9.8±1.1	10±0.3	13±1.7	6.3±0.9	2.8±0.3	6.9±2.9
MSOC/TC[c]	82±2.2	88±1.5	57±11	53±7.5	78±16	52±27	99±0.2	95±1.9	98±0.1	96±0.1	95±1.8
HULIS-C/WSOC[c]	64±6.9	65±8.0	42±6.2	43±5.4	41±6.6	32±6.3	41±4.9	46±9.4	46±9. 6	43±6.0	33±7.8
WSOC/OC[c]	23±5.9	23±3.1	33±0.9	24±4.0	36±2.6	35±3.2	25±2.9	30±4.5	14±3.3	6.4±0.5	26±3.9
HULIS-C/OC[c]	15±2.9	15±0.4	14±1.7	10±0.7	15±1.9	11±3.2	10±0.3	13±1.6	6.4±0.9	2.8±0.3	6.9±3.0
MSOC/OC[c]	88±1.9	91±1.2	70±4.5	76±2.5	72±6.7	77±4.5	99±0.1	96±0.5	98±0.1	98±0.5	96±1.6

[a] Total Carbon: sum of OC and EC

[b] The ratios of the mass of carbon (μgC) to the mass of PM (μg) for each sample.

[c] The ratios of the mass of carbon (μgC) to the mass of carbon (μgC) for each sample.

Table 2. The proton species in the BrC fractions (WSOC, HULIS, and MSOC) of smoke samples.

		WSOC				HULIS				MSOC			
	Samples	R-H	H-C-C=	H-C-O	Ar-H	R-H	H-C-C=	H-C-O	Ar-H	R-H	H-C-C=	H-C-O	Ar-H
		0.6-2.0 [a]	2.0-3.2	3.4-4.4	6.5-8.5	0.6-2.0	2.0-3.2	3.4-4.4	6.5-8.5	0.6-2.0	2.0-3.2	3.4-4.4	6.5-8.5
Biomass burning	WS	16[b]	27	42	14	19	32	21	27	44	26	16	14
	RS	24	27	34	14	26	31	14	29	46	30	13	11
	CS	15	22	46	17	18	28	31	24	47	29	15	9
	PW	14	22	48	17	15	25	42	18	40	30	19	11
	CF	11	17	54	18	14	26	36	23	41	28	18	13
	WP	12	22	48	19	14	21	31	34	44	29	17	10
Coal combustion	B-1	18	41	9.0	32	17	40	5.0	37	40	28	2.0	30
	B-2	17	35	22	25	26	39	5.0	30	33	30	3.0	33
	B-3	17	39	14	30	22	34	8.0	35	34	30	2.0	33
	B-4	13	27	34	25	20	36	13	30	32	27	3.0	39
	AN	15	33	20	32	18	37	12	33	38	28	2.0	32

[a] chemical shift: ppm. [b] percentage of each type of protons (%).

Table 3. Pearson correlation coefficient analysis between oxidation potential and chemical characteristics of BrC

	DTT_c[a]	
	R	p
MAE_{365}	0.697**	0.000
Fluorescence component 1 (%)[b]	-0.078	0.668
Fluorescence component 2 (%)[b]	-0.330	0.061
Fluorescence component 3 (%)[b]	0.151	0.402
Fluorescence component 4 (%)[b]	0.560**	0.001
R-H (%)	0.697**	0.000
H-C=C (%)	-0.247	0.166
H-C-O (%)	-0.223	0.213
Ar-H (%)	-0.345*	0.049

a: DTT_c were calculated using the DTT consumption rate divided by the mass of organic carbon.

b: fluorescence component 1-4 poresent fluorophores 1-4 (C_W1-4 and C_M1-4) identified by PARAFAC method

** There was significant correlation in 99% confidence interval (bilateral) (p value no more than 0.01).

* There was significant correlation in 95% confidence interval (bilateral) (p value no more than 0.05).

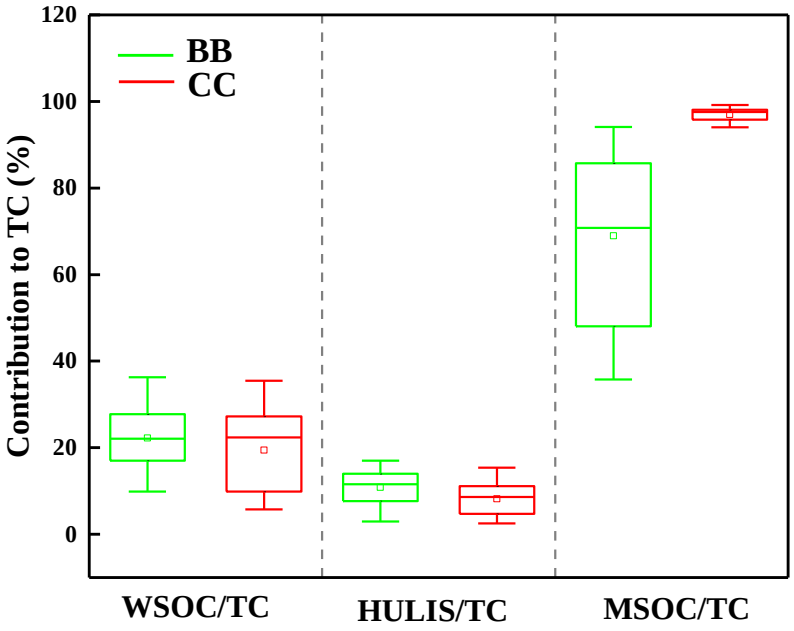

Figure 1. The abundances of BrC fraction in the smoke samples from biomass burning (BB) and coal combustion (CC)

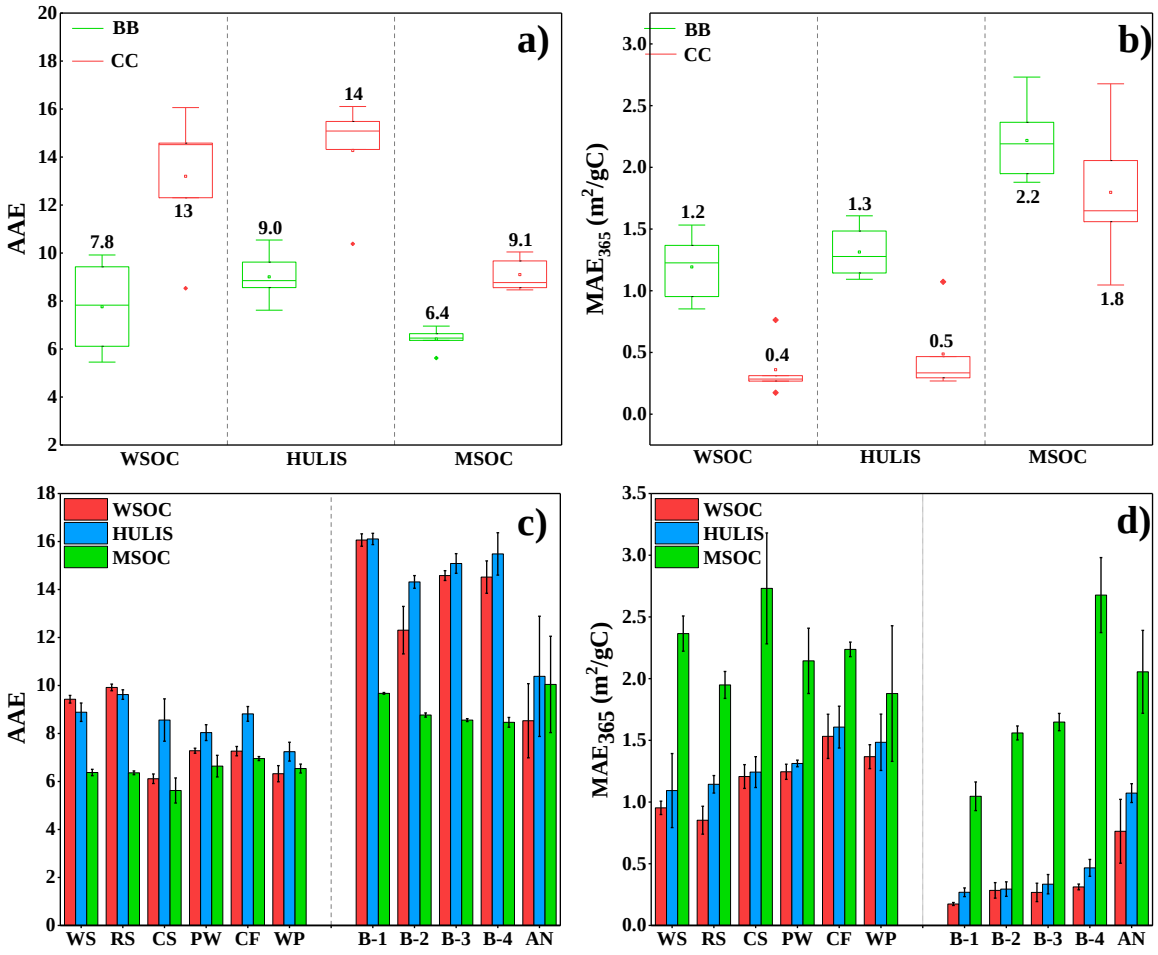

Figure 2. The AAE and MAE_{365} values of WSOC, HULIS, and MSOC in smoke samples from biomass burning (BB) and coal combustion (CC)

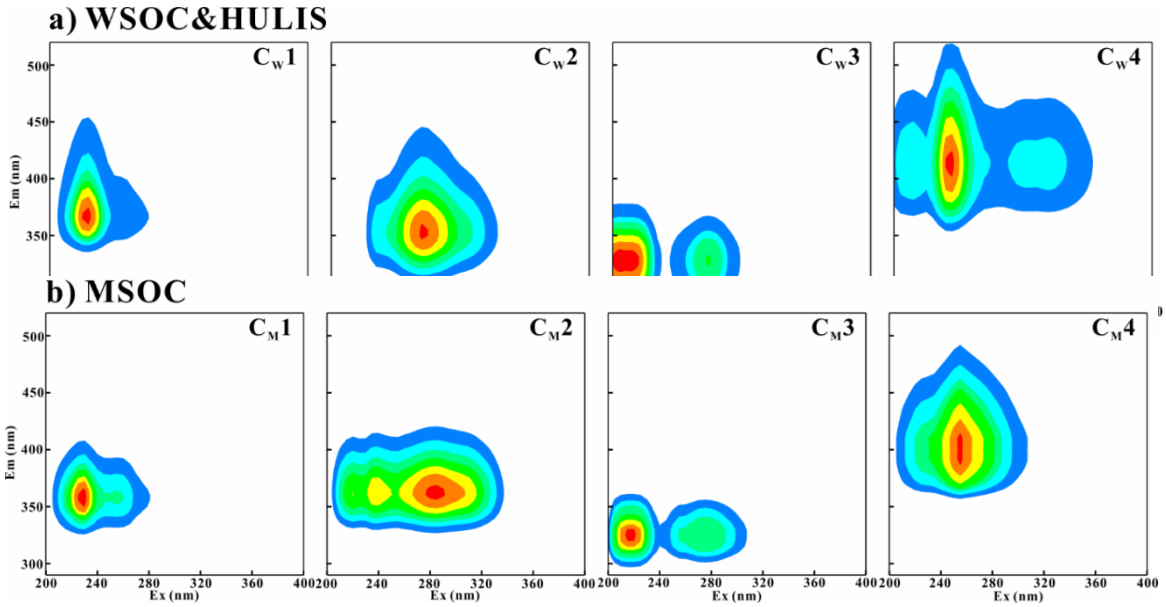

Figure 3. Four fluorescence components identified by PARAFAC analysis of a) WSOC, HULIS (C_W1:C_W4); b) MSOC (C_M1:C_M4) extracted from BB and CC smoke $PM_{2.5}$ (normalized in Raman unit, R.U.)

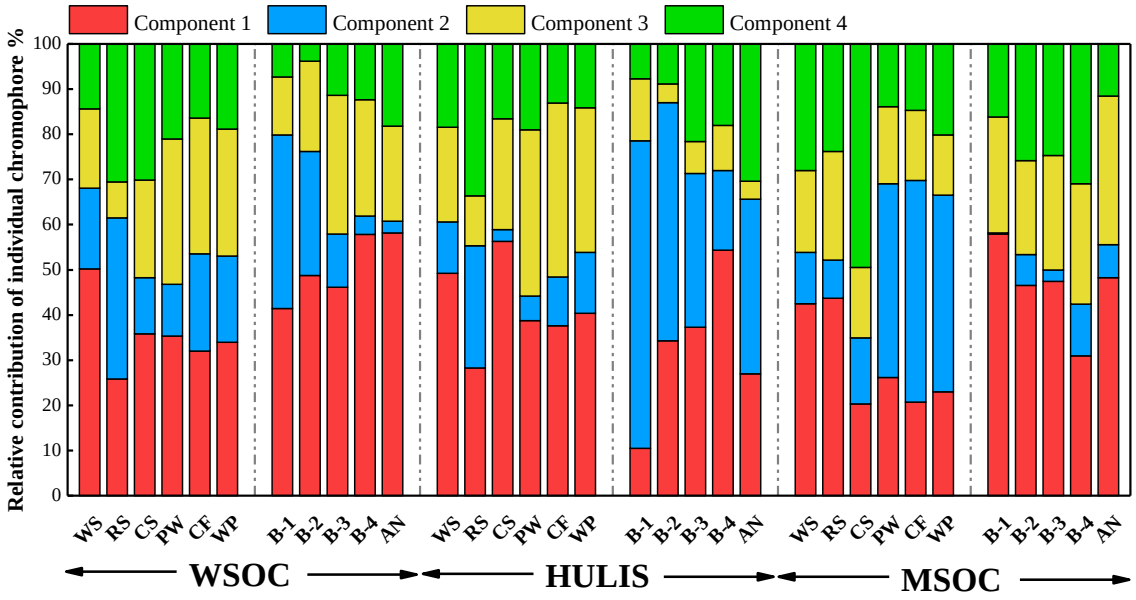

Figure 4. Relative contribution calculated by F_{max} of individual chromophores analyzed by PARAFAC. Component 1-4 represent C_W1-4 for water-soluble BrC (WSOC and HULIS) and and C_M1-4 for methanol-soluble BrC (MSOC), respectively.

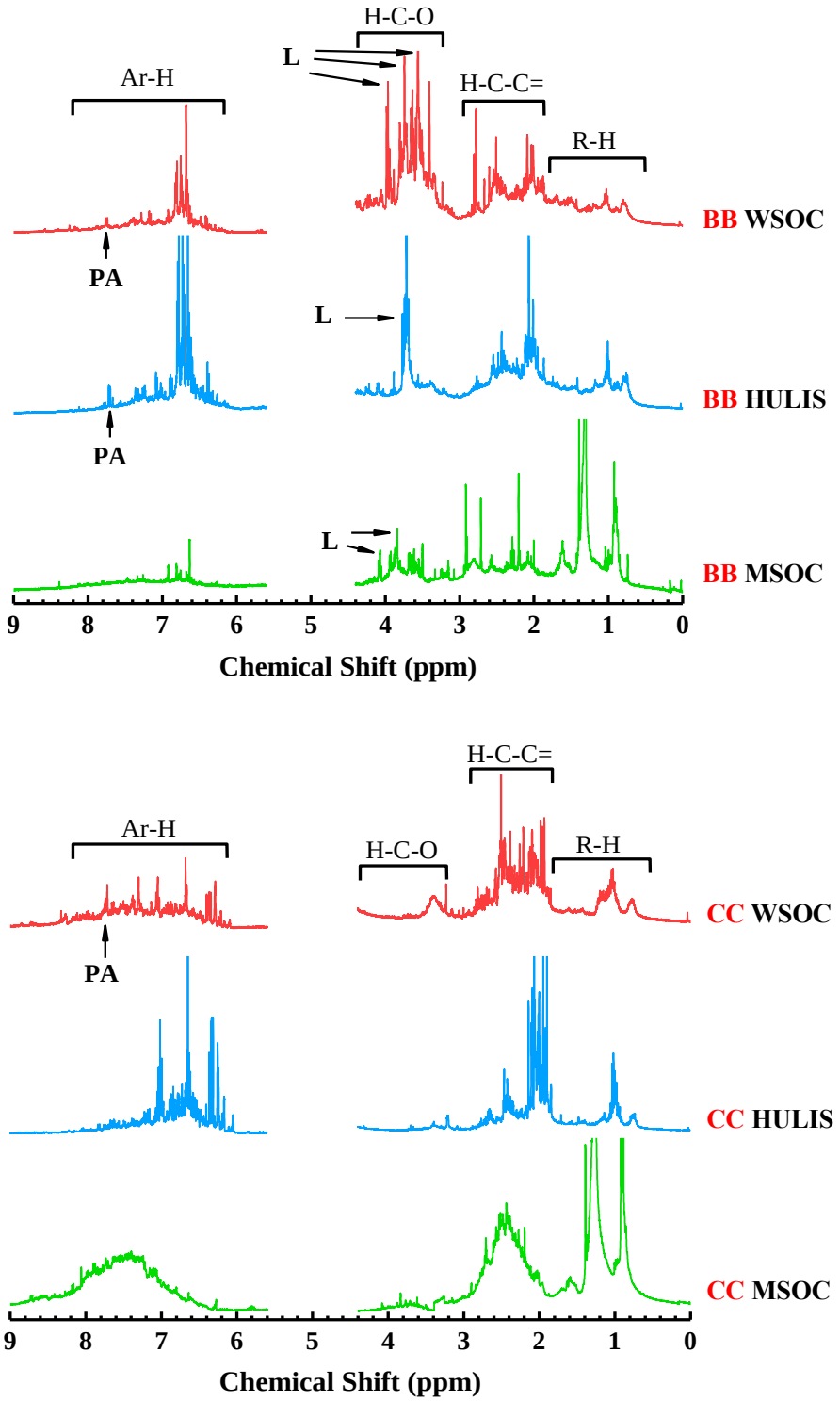

Figure 5. ^{1}H NMR spectra of WSOC, HULIS, and MSOC in typical biomass burning and coal combustion smoke samples (BB: wheat straw; CC: B-1 coal). The segment from 4.40 to 5.60 ppm was removed for NMR spectra due to MeOH and H_2O residues. The peaks were assigned to specific compounds as follows: Levoglucosan (L), Phthlic acid (PA).

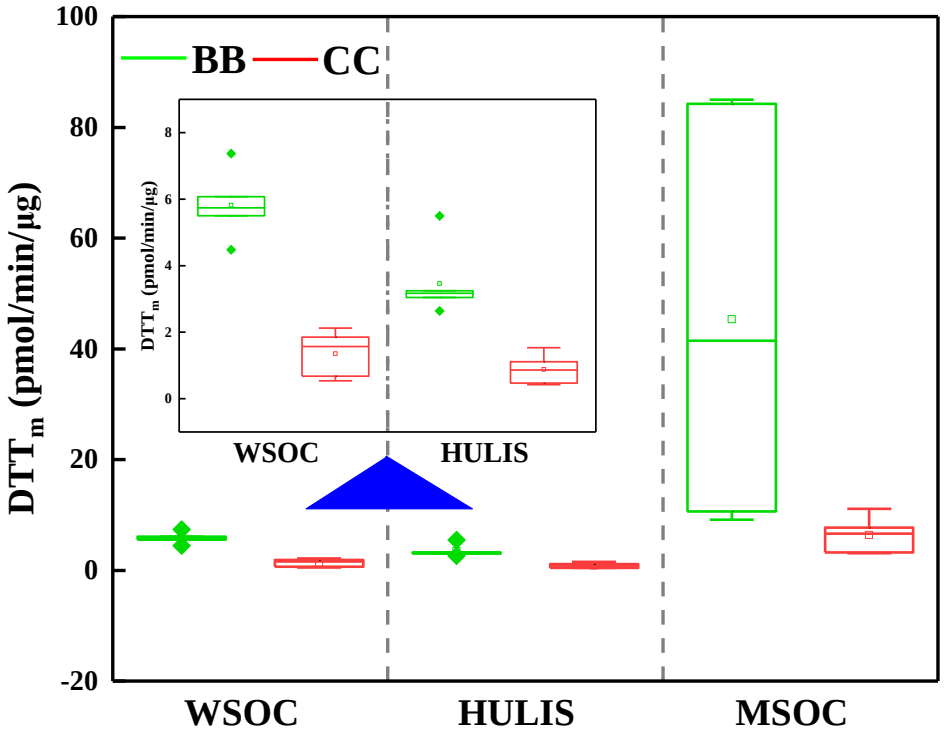

Figure 6. Results of DTT assay conducted on the WSOC, HULIS and MSOC of smoke $PM_{2.5}$, the values were normalized by the mass of smoke $PM_{2.5}$. Above the blue triangle symbol is the result coordinates of WSOC and HULIS to be enlarged.

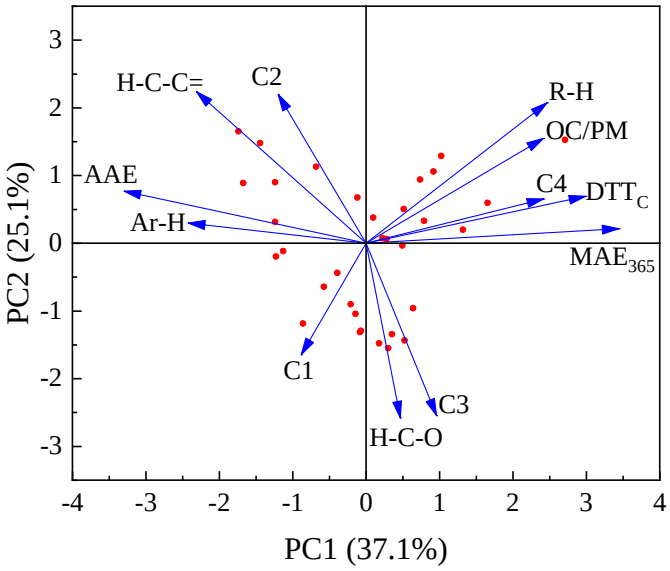

Figure 7. Principal component analysis results for the carbon mass-normalized OP activities and chemical characteristics of BrCs in smoke particles.